SPECTRA OF DIVALENT RARE EARTHS IN CALCIUM FLUORIDE AND CALCULATION OF ENERGY LEVELS OF THE f^6 AND f^8 CONFIGURATIONS IN INTERMEDIATE COUPLING

By

WILLIAM BECKHAM VOLZ

Bachelor of Science

Oklahoma State University

Stillwater, Oklahoma

1963

Submitted to the Faculty of the
Graduate College of the
Oklahoma State University
in partial fulfillment of
the requirements for
the Degree of
DOCTOR OF PHILOSOPHY
May, 1970

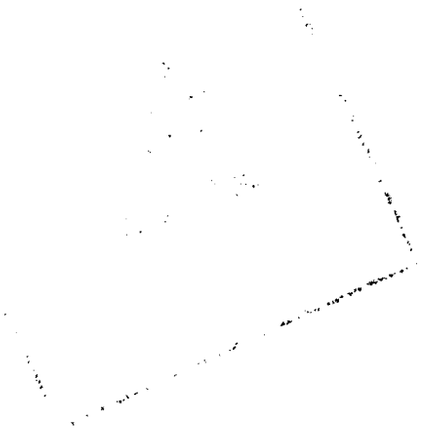

SPECTRA OF DIVALENT RARE EARTHS IN CALCIUM FLUORIDE AND CALCULATION OF ENERGY LEVELS OF THE f^6 AND f^8 CONFIGURATIONS IN INTERMEDIATE COUPLING

Thesis Approved:

Louis P. Varga
Thesis Adviser

J. Paul Davis

E. E. Koch

Horacio A. Moffola

D. Durham
Dean of the Graduate College

PREFACE

This dissertation is concerned with the study of the divalent oxidation state of the lanthanides. Divalent cerium, praseodymium, gadolinium, holmium and erbium ions in single-crystal calcium fluoride have been produced by the techniques of irradiative and electrolytic reduction, and their absorption and emission spectra have been obtained. The available information in the literature on the energy levels of divalent lanthanides has been used to obtain the variation of the electrostatic and spin-orbit coupling parameters with the number of electrons in the 4f shell. The intermediate coupling diagrams of the seven lowest and seven highest terms of the f^6 and f^8 configurations have been constructed. The diagrams illustrate the change in the positions of the energy levels for the change from Russell-Saunders to jj coupling.

I would like to express my gratitude for all the assistance and interest expressed by the members of my committee: Dr. L. P. Varga, Dr. H. A. Mottola, and Dr. J. P. Devlin of the Chemistry Department and Dr. E. E. Kohnke of the Physics Department.

In addition, I would like to thank Mrs. LaVerne Cook for typing, Mr. Mack Crank for preparation of the figures,

and Dr. George Gorin for irradiation of the crystals.

Finally, the understanding and sacrifice of my wife, Cheryl, has made it possible for me to obtain this degree.

TABLE OF CONTENTS

LIST OF TABLES

LIST OF FIGURES

CHAPTER I

INTRODUCTION

This study was originally designed to be an extension of some work done on the divalent lanthanides in calcium fluoride, the divalent states of cerium (f^2), praseodymium (f^3), holmium (f^{11}), and erbium (f^{12}) were to be studied. These configurations were selected because their energy levels could be least-squares fitted within a reasonable amount of computer time. Divalent gadolinium was also to be examined because there was some uncertainty in the literature about whether its ground state was f^8 or f^7d.

As originally outlined, the program consisted of production of calcium fluoride single crystals, doped with the various lanthanides at low concentrations, reduction of the trivalent lanthanides to the divalent state by solid-state electrolysis at high temperatures, and examination of the absorption and fluorescence spectra of the lanthanide ions in the reduced state. That portion of the spectra which could be attributed to the f-f transitions of the divalent ions was to be fitted by least-squares computer techniques to the theoretically predicted spectra in order to obtain the electrostatic and spin-orbit coupling parameters, which were then to be compared to

the isoelectronic trivalent ions to determine trends in their variation with the number of electrons in the configurations. If the data for the divalent ions were good enough, a study of the crystal-field splitting of the levels was also to be done, in order to obtain information on the environment in which the divalent ions in the crystal were situated.

All of the original goals in the study were not accomplished. No single crystals were grown in the laboratory because some mechanical or electrical defect in the induction furnace which was to be used for the growth of the crystals prevented the graphite crucibles from reaching a high enough temperature to melt more than a very small quantity of calcium fluoride. Single crystal chips of doped calcium fluoride were obtained from a commercial source, and were somewhat less than ideal. Some of them contained impurities, and, since they were small, a good deal of difficulty was encountered in mounting them in the holder for electrolysis. One of the crystals was found to be unstable to heat, rendering it useless for reduction purposes. The solid-state electrolysis procedure was complicated by the deposition of calcium in the crystal. This resulted in only localized reduction of the lanthanide ions in a small volume of the crystal near the calcium dendrites, with a consequent reduction in the number of divalent ions available for study. Because of the difficulties encountered with the solid-state

electrolysis procedure, a second group of crystals were purchased from the same source for reduction by exposure to ionizing radiation. No difficulties were encountered with the crystals used in this procedure except the anticipated one of instability of the divalent state to light and heat. Due to the low concentration of divalent ions produced by either of the two methods, no f-f absorption or fluorescence lines were observed which could be attributed to the divalent lanthanides, with the possible exception of gadolinium. It was found that the lone fluorescence line observed for this ion could be adequately explained by assumption of the f^8 configuration and reasonable values of the parameters used to describe the theoretical spectrum. However, the presence of previously undetected impurities as the source of the observed fluorescence could not be completely ruled out. As a result of the lack of observed absorption or emission lines, no crystal-field studies were attempted.

The part of the study dealing with the observation of trends in the variation of the electrostatic and spin-orbit parameters with the number of electrons enjoyed a somewhat greater degree of success. Using literature values for the free-ion spectra of Ce III, Pr III, and Ho III, values for the electrostatic and spin-orbit parameters were computed and compared graphically to those for the trivalent cases. The plot of the spin-orbit parameter versus the number of electrons in the 4f shell was then used to obtain

a value for divalent gadolinium. Using this value, the electrostatic parameter was then varied until a fit was achieved for the parent level of the observed fluorescence line of gadolinium.

The intermediate coupling diagrams for the seven lowest and seven highest multiplets of both the f^6 and f^8 configurations were constructed by use of literature values of the electrostatic and spin-orbit parameters for some of the points on the diagrams. For other points, assumed values of the two parameters which were consistent with the theory were used to obtain enough information for construction of the figures. It is hoped that these figures will prove useful to other investigators.

Appendix A describes some previous studies and their results. The first part deals with some calculations which were performed for the purpose of obtaining self-consistent radial wave functions of some of the lanthanide ions. The second part outlines the construction and use of a ruby laser as a light source for Raman spectrography. Appendix B consists of the major results of this study, compiled in a form which is suitable for submission to a journal for publication.

One choice of notation should be explained. The so-called spectroscopic notation of the degree of ionization of an element is given by the symbol for the element followed by a Roman numeral indicating the ionization. If the observed spectrum arises from the unionized atom, say

potassium, then the symbol for this spectrum is K I. If it is singly ionized, the symbol is K II. Chemical notation consists of the symbol for the element, followed by a Roman numeral, enclosed in parentheses, which indicates the degree of ionization. Therefore, singly ionized potassium, in chemical notation, is K(I). In this study, if the free-ion spectrum, either observed or calculated, is under consideration, spectroscopic notation will be used, while if an observed spectrum of an ion in a condensed phase, such as an ion in a crystal, is being considered, chemical notation will be used. For example, the free-ion spectrum of divalent samarium will be denoted Sm III, while the spectrum of divalent samarium in a crystal or a solution will be Sm(II).

Literature Review

The study of the lanthanides has increased since separation techniques have improved to the point that pure compounds of each of the elements of this series have become available at reasonable prices. This family of elements is almost unique in that the members have very similar chemical properties. Conversely, an outstanding diversity in their spectroscopic properties provides a most convenient method for the study of the differences between individual members and the trend of chemical and physical properties within the family. Spectroscopic studies have provided important tests of the theory of

electronic spectra which finds immediate application in the study both of lanthanide and actinide compounds.

An early review of the spectroscopic properties of the lanthanides is that of Dieke and Crosswhite (1), in which they outline the work done at Johns Hopkins University and elsewhere on the various oxidation states of the lanthanides in crystals and as free ions. A much more extensive compilation of data on the lanthanides in crystals is that of Dieke (2), which contains discussions of the types of crystals available for study, the various experimental techniques involved, and the methods of comparing experimental information to that predicted by the theory. The book also contains a compilation of the available data on the low-lying levels (0 to approximately 50000 wave numbers) of all the rare earths except promethium. There is also a table of the observed fluorescence lines of all the rare earths in $LaCl_3$.

Wybourne's book (3) contains a discussion of the theory behind the observed absorption and emission lines arising from the f-f electronic transitions of the lanthanides. The book by Sinha (4) contains extensive information on the chemical and physical properties of all the lanthanides, but special emphasis is placed on europium. Asprey and Cunningham (5) review some of the early work on the less stable oxidation states of both the lanthanides and the actinides. Fong (6) discusses the various techniques and the theory behind them for production of

the divalent lanthanides as impurities in calcium fluoride. He also deals with the general subject of color centers in the various alkaline earth halides, discusses the processes by which they are formed and the influence of impurities on the optical behavior of the crystals. The paper by Carnall and Fields (7) discusses the spectra of the trivalent lanthanides and actinides in solution and tries to predict the trends of the parameters used to fit the observed spectra. The observed intensities of the f-f electronic transitions are compared to those calculated in the paper.

Several papers have been published on the production of the divalent lanthanides in various ionic crystals. The earlier work was done on natural crystals, such as fluorite, in which the lanthanides are found at impurity levels because of similarities between their ionic radii and that of the cation in the host lattice. One of the earliest papers on synthetic calcium fluoride doped with the lanthanides was that of McClure and Kiss (8). They give the absorption spectra of the divalent rare earths obtained by exposure of the crystals to gamma radiation, and some fluorescence lines which are attributed to f-f electronic transitions between the low-lying states. They give the results of a calculation for each of the ions in which an approximation to the excitation energy from the f^n configuration to the lowest $4f^{n-1}5d$ level is obtained. The calculated energy difference is compared

to that represented by the onset of the observed broad-band absorption, after the calculated values have been adjusted so that an exact fit for divalent samarium is achieved. A fairly good fit is obtained for all the cases considered except for cerium, gadolinium, and terbium. They interpret this as indicating that there is a possibility that the $4f^{n-1}5d$ configuration is the ground state.

Two papers by Merz and Pershan (9) illustrate a slightly different type of study which can be done with the divalent lanthanides in alkaline earth halides. In the study described in these papers, the lanthanides are reduced to the divalent state by exposure to gamma radiation or x-rays at 77°K, then the crystals are warmed up slowly and the light emitted by the recombination of electrons and holes from the various types of traps in the crystal is monitored. Both the total amount of light emitted as a function of temperature and the spectral distribution of the light are studied. When a hole recombines with the electron trapped at a divalent rare earth, this leaves the rare earth in an excited state, and the fluorescence observed is characteristic of the trivalent ion. Two results obtained by this technique are that the thermoluminescent glow peaks are independent of the rare earth dopant, indicating that the types of traps are the same for each ion, and that the composition of the thermoluminescent emission is characteristic of the trivalent ion in a cubic site. The second result is obtained from

a crystal-field analysis of the emission lines which are intense enough for such a study. For emission above room temperature, the site symmetry of the lanthanide ion was found to be tetragonal. Hayes and Twidell (10) and Sabisky (11) conducted paramagnetic resonance studies on thulium and holmium, and holmium, respectively, and conclude that only ions at cubic sites are reduced by ionizing radiation. A paper by Kariss and Feofilov (12) gives the references for the Russian work on the divalent lanthanides in the alkaline earth halides.

The study of the free ion spectra of the lanthanides is only partially complete at the present time. Dieke and Crosswhite (1) give a table containing the number of levels for the four lowest configurations of the trivalent rare earths, and a partial list of the allowed transitions between the levels. While the numbers are fairly small for the members at each end of the series, they increase rapidly as the number of f electrons increases. In their paper, they show rough diagrams of the third and fourth spectra of the lanthanides, and the observed levels of the trivalent ions in various crystals. Odabasi (13) has published a partial list of observed lines of La III, and has assigned some levels for about 20 configurations. The assignments are rather simple, since only one electron outside of a closed shell is involved. Sugar (14) has reported the emission spectrum of Ce III and has concluded that the ground state of the free ion is the $4f^2$

configuration, but also found that the lowest level of the 4f5d configuration is only about 3300 wavenumbers above that of the ground state. Trees (15) reported 38 of 41 possible levels of the $4f^3$ configuration of Pr III, and found this to be the ground state configuration. The lowest level of the $4f^25d^1$ configuration was found to be some 31000 wavenumbers above the ground state. Dupont (16) reported the ground multiplet of the $4f^6$ configuration and some lines of the $4f^55d^1$ configuration of Sm III. McElaney (17) made a partial analysis of the $4f^{11}$, $4f^{10}5d^1$, $4f^{10}6s$, and $4f^{10}6p$ configurations of Ho III. The $4f^{11}$ configuration was found to be the ground state and the levels reported included the ^4I multiplet, the $^4F_{9/2}$ level, and the $^2H_{11/2}$ level. The lowest levels of the $4f^{10}6s$ and $4f^{10}5d$ configurations were found about 20000 wavenumbers above the ground state. Callahan (18) identified the ground state of Gd III as $4f^75d^1$ and found all the levels for this configuration, as well as those for the $4f^76s$ and $4f^76p$ configurations. He did not observe any levels of the $4f^8$ configuration, and stated that these must lie less than 10000 wavenumbers from the upper half of the $4f^75d$ configuration. Finally, Bryant (19) has performed an analysis of both the third and fourth spectra of ytterbium.

Varga and Asprey (20) describe one version of a computer program used to calculate the energy of the f^n configuration of the lanthanides and actinides. The program

uses the coulomb and spin-orbit matrices for f electrons calculated by Nielson and Koster (21). Two other types of calculations which have proven useful for studies of the lanthanides are those by Freeman and Watson (22) and Herman and Skillman (23). The first uses the Hartree-Fock approximation in the calculation, while the second reference uses the Hartree-Fock-Slater self-consistent field approach.

The previously mentioned review articles contain many references to the spectra of lanthanides in the alkaline earth halides and other salts. The paper by Wood and Kaiser (24) on the absorption and fluorescence of Sm(II) in CaF_2, SrF_2 and BaF_2; one by Loh (25) on the ultraviolet absorption spectra of Ce(III) in alkaline earth fluorides; the paper by Rabbiner (26) on the cubic crystal field levels of Tb(III) in CaF_2; and the section of Judd's book (27) on the problem of intermediate coupling will all be considered in some detail in the discussion of the results of research performed for this thesis.

CHAPTER II

THEORETICAL ASPECTS OF RARE EARTH SPECTROSCOPY

The number of possible terms which arise for a given configuration is characteristic for that configuration. That is, a single electron or hole in the f shell gives rise to a single term; two electrons or holes give rise to seven terms, and so on. Furthermore, these terms are themselves degenerate and will give rise to a number of levels, whose designation is dependent on the particular coupling scheme which holds for the case under consideration.

The scheme which holds in most cases for the lanthanides is called LS or Russell-Saunders coupling. In this scheme, the individual orbital angular momentum of each electron in the f shell adds vectorially to give the total orbital angular momentum, L. Likewise, the total spin, S, is the vector sum of the individual spins. The quantity (2S+1) is called the multiplicity of the term, and is written to the left of the total angular momentum as a superscript. The standard notation for a term with L = 0, 1, 2, 3, 4, 5, . . . is S, P, D, F. G, H, . . . so that a term is represented as ^{2S+1}L. One further quantity, J, needs definition. J is the vector sum of S and L and

the spin-orbit interaction removes the degeneracy of the levels of varying J-values within a term. When $L \geq S$, J takes on the values L-S, L-S+1, . . . , L+S; when $L < S$, J takes on the values S-L, S-L+1, . . . , S+L. Therefore, the designation of an individual level is $^{2S+1}L_J$. As more electrons are added to the f shell, the number of terms with the same S and L increases and other quantum numbers have to be introduced in order to properly label the levels.

Electrostatic interactions between the electrons within the f shell serve to produce the various terms within a particular configuration. The centers of gravity of these terms can be expressed (4) as multiples of the F^k integrals,

$$F^k = e^2 \int_0^\infty \left[\int_0^{r_2} (r_1^k / r_2^{k+1}) R^2 dr_1 + \int_0^\infty r_2^k / r_1^{k+1}) R^2 dr_1 \right] R^2 dr_2$$

where e is the electronic charge, R is the radial wave function, and k takes on the values 2, 4, and 6. A simplification to remove large denominators consisted of redefinition of the F^k integrals as $F_k = F^k / D_k$ where, for the f-shell, $D_2 = 225$, $D_4 = 1089$, and $D_6 = 7361.64$.

An alternate method of expressing the behavior of the f^n configuration is in terms of the Racah parameters, E^i. They arise from the application of group theoretical techniques to the problem of calculation of the energy matrices

of the f^n configuration. Judd (27) explains the similarities and differences between the two techniques.

In both cases, the expression for the energy matrices of the f^n configuration is written as a linear combination of either the E^i or the F_k. There is a linear relationship between the two sets of parameters of the form

$$F_0 = 1/7\ (7E^0 + 9E^1)$$

$$F_2 = 1/42\ (E^1 + 143E^2 + 11E^3)$$

$$F_4 = 1/77\ (E^1 - 130E^2 + 4E^3)$$

$$F_6 = 1/462\ (E^1 + 35E^2 - 7E^3)$$

Rearrangement of these expressions yields a similar set for obtaining the Racah parameters as a function of the F_k. The coefficient of both E^0 and F_0 in the energy summation depends only on the number of electrons in the configuration, so it only serves to shift the whole configuration, without changing the relative positions of the terms. Therefore, it is usually not considered when a single configuration is under study, and the usual practice is to subtract it off, setting the lowest level equal to zero.

In obtaining the energy levels of the lighter atoms, it has been found sufficient in most cases to consider purely electrostatic interactions. As the size of the atom increases, other effects, such as spin-orbit, spin-spin, and spin-other-orbit types of magnetic interactions

must be included. The first of these, spin-orbit, is the largest of these effects. The matrix elements must be expressed as linear combinations of both the electrostatic and spin-orbit parameters. The inclusion of the effect of spin-orbit splitting causes the levels which belong to different terms, but with the same value of J, to become mixed, thus S and L have little meaning as far as the identification of the levels is concerned, since a level may be comprised of three or four terms of about equal percentage composition. This effect is not too bad near the ends of the 4f shell, but around the middle when the number of levels is the greatest, it is quite noticeable. It is probably also evidenced in the large scatter in the values for F_2 that different investigators have found for the ions in this region. For instance, Carnall and Fields' (7) values for F_2 show nearly linear behavior from the first of the series up to samarium, then for europium, gadolinium, and terbium the values are about 25% higher than the value for samarium. After these three, a drop is taken, and the rest of the series finishes out at about the same rate of increase as the first members. On the other hand, the change in the values for F_2 is barely noticeable in the table given by Sinha (4) or Dieke (2).

When the data are not too good, or when only low precision is desired, it has been found useful to assume that the 4f-radial eigenfunctions are hydrogenic in nature and to express F_4 and F_6 in terms of F_2. The hydrogenic

ratios are given by the two expressions, $F_4/F_2 = (41/297) = 0.13805$ and $F_6/F_2 = (7 \times 25/81 \times 143) = 0.01511$. As was previously mentioned, the effect of the other magnetic interactions, spin-spin and spin-other-orbit, while small, grow increasingly important as the level of accuracy desired is increased, and as the values for the terms which lie at higher values are calculated. At these energies, the effect of the electrostatic interactions between the f^n configuration and higher configurations of the same parity may also become important. These areas have not yet been studied in any great detail, but a start has been made with a pair of papers (28, 29).

The first paper obtains the matrix elements for spin-spin and spin-other-orbit interactions for the f^2 configuration in terms of three radial integrals, M^k, which are more or less analogous to the Slater integrals. The introduction of these parameters produced a substantial reduction of the mean error for two f^2 cases, Ce III and Pr IV. Improvements in fit were also noted for calculations on the low-lying sextets of Pm I(f^5) and Gd IV(f^7).

The second paper takes a slightly different approach with the f^3 configuration. Substantial reductions in the error for the case of Pr III is obtained by the introduction of a group of effective operators which can be made to represent not only the various types of magnetic interactions, but also configuration interactions of certain kinds. The results were then used to obtain improvements

in the fit for Nd(III) and Er(III) in $LaCl_3$. In both papers, pure Russell-Saunders coupling was assumed to hold.

The computer program used in this work originated at the Lawrence Radiation Laboratories and was modified at Argonne National Laboratories (ANL Program 1849/CHM 177) and at Oklahoma State University by L. P. Varga in 1967. The least-squares routine was added by Bob Ryan at Los Alamos in 1967. Since then, the program has been further modified in small ways both by L. P. Varga and myself. The program uses a tape of the Racah coefficients of energy matrices for the f^n configuration prepared at MIT by Nielson and Koster (21) and modified at Lawrence Radiation Laboratories. The tape requires a maximum of six parameters for the f^2 case, and up to ten for the f^3 configuration.

The program is controlled by 14 parameters which are read in at the start. They allow the program to determine whether F_2 and Zeta, the F_k and Zeta, or the E^i are to be used in the calculation of the energy levels. Others determine whether experimental levels are fitted, and whether or not the least-squares subroutine is to be used. Two parameters are read in which define the weighting of the levels and the rate at which the E^i are varied. A second card is read which defines the number of electrons in the configuration, the number of J-manifolds under consideration, and the J values in halves with the ground state first and the others in ascending order. The trial values of the parameters used in the calculation are then read in.

The E^i are read in directly; if the hydrogenic approximation is assumed, F_2 is multiplied by the hydrogenic ratios times the factors in the linear relationship which converts the F_k into the E^i. For the lanthanides, these factors are

$$E^1 = 14.6818 \times F_2$$

$$E^2 = 0.07685 \times F_2$$

$$E^3 = 1.4845 \times F_2$$

When the F_k are read in, they are converted by the following expressions

$$E^1 = 1/9\ (70 \times F_2 + 231 \times F_4 + 2002 \times F_6)$$

$$E^2 = 1/9\ (F_2 - 3F_4 + 7F_6)$$

$$E^3 = 1/3\ (5F_2 + 6F_4 - 91F_6)$$

If experimental levels are to be fit, they are read in next, in increasing magnitude in units of wavenumbers. They are assigned numbers within each J-manifold which determine the levels to which they correspond.

The Ryan subroutine is then called if the E^i are to be varied in the calculation. Using the parameters which were read in at the start of the program, the energy matrices for each value of J are built up by multiplication of the proper Racah parameters by the coefficients read from the tape and by summation in the proper manner. The arrays are then diagonalized to obtain the first values

for the energy levels. This procedure is then repeated after a small variation in the Racah parameters. The differences between the two sets of calculated energy levels, divided by a weighted value of one of the Racah parameters, are calculated, as are the differences between the observed and calculated energy levels. The sum of the weighted squares of the differences between observed and calculated energy levels is also calculated. A calculation then follows which results in a new set of E parameters. This involves construction of a matrix from the various error parameters. This array is inverted and multiplied by a vector whose elements depend on the weighted deviations between the observed and calculated energy levels and the deviations between two sets of calculated energy levels. The resultant vector is multiplied by the damping factor and its elements are added to the previous set of E's.

At this point, the sum of the weighted squares of the differences between observed and calculated energy levels is compared to the same quantity from the previous cycle. If subtraction of the current value from the previous value produces a positive quantity which is greater than or equal to the previous value multiplied by 10^{-4}, the cyclic process continues. When either one of these conditions is violated, or when the maximum number of cycles has been completed, control is returned to the main program.

The main program calculates and prints the F_k values and calls the CHM/177 subroutine. This subprogram calculates the intermediate coupling parameters and, using the final set of E's, generates the energy matrices and the final set of calculated energy levels. The final output is prepared and printed and control is returned to the main program. Calculation of another case, if one is desired, is then begun.

CHAPTER III

THE INTERMEDIATE COUPLING PROBLEM

Candler (30) states that the interaction between an ion and an electron can be represented by the method of combination of four vectors, the orbital vector of the ion, that of the electron, the spin vector of the ion, and that of the electron. Four types of interactions between these vectors should be considered. These are, the response of the spin of the ion to that of the electron, the behavior of the two orbital vectors with respect to one another, the interaction between a spin vector and its own orbital vector, and finally, the interaction between a spin vector and another orbital vector. Of these four, usually only the first three are considered.

Let us now consider an ion (or atom) with a partially filled shell. Each electron in the shell will have a spin vector, s_i, and an orbital vector, l_i, associated with it. The s_i have only two allowed values, $\pm\frac{1}{2}$, while the l_i values are dependent on the partially filled shell under consideration. If the spin vectors are added vectorially to form a resultant, S, and if the orbital vectors are combined in the same fashion to form a resultant, L, then this method of combination is known as Russell-Saunders or

LS coupling. L and S are combined vectorially to form another quantity, J, the total angular momentum vector. Since the allowed values of s_i and l_i are determined, for a particular shell, by the number of electrons in the shell, combining the electronic vectors in this fashion produces a set of S, L and J values which are characteristic of each configuration.

For Russell-Saunders coupling, the interaction of the spins has the effect of dividing the terms, which are identified by a particular S and L value, into groups, all the terms of which have the same S value. The terms with the maximum possible S value for a configuration usually lie the lowest. For a set of terms of the same S value, the maximum value of L will lie the lowest. This behavior is a result of the interaction of the orbital vectors. Within a single term, the maximum value of J lies the lowest for configurations in which the shell is less than half full, and highest for shells which are more than half full. The interactions between the s_i and the l_i can also be considered as coulombic interactions, while the one between a single electron's s and l values is magnetic.

For the lighter elements, particularly those on the left side of the periodic table, the coulombic interactions are the predominant factors in the determination of the structure of the emission spectra. For these ions in crystals, the absorption or emission spectra are determined by a combination of coulombic and crystal field

effects. The spin-orbit interaction for most free ions in this class is seen as a splitting of the terms which is small in comparison to the energy difference between the terms. Since one of the effects of the crystal field is a broadening of the free ion levels, the spin-orbit interaction is not observed for this family of ions in the solid state or in solution. As atomic weight increases, there is a generally increasing breakdown of Russell-Saunders coupling, starting first with the higher terms of a spectrum. Even for an element as light as argon, the breakdown has progressed to such an extent that values of S and L cannot be assigned to the observed levels (30).

Of course, the whole point of observing the spectra of ions in the free state or in some condensed phase is to enable the researcher to develop a theory which will allow him to predict the position of levels in a new system which he wishes to study. As far as calculations based on theory are concerned, the effect of breakdown of Russell-Saunders coupling evidences itself in several different ways. One of these is that different levels of the same J-value are mixed, so that levels no longer retain their identity. An immediate effect of this is that selection rules for allowed transitions, which are either theoretically predicted or empirically found to hold for LS coupling, are apparently violated due to the levels having mixtures of terms for which the selection rules are valid. The Lande

interval rule states that the splitting between two levels of a given term is proportional to the higher J-value of the two levels. This rule is followed for LS coupling, and has been quite useful in identification of the members of a term, but as deviations occur it becomes invalid. The g-factor also behaves in a similar fashion, i.e. the observed and calculated g-factors agree quite closely for spectra which are well represented by LS coupling, but as breakdown occurs, the g-factors may deviate. These and other inconsistencies which have been interpreted in terms of LS breakdown do not necessarily occur at the same time. The observed g-factors may agree quite closely with calculated ones while the interval ratios are abnormal. No matter how abnormal a spectrum is, the J values for the configuration remain the same (30).

The absorption spectra for the common valences of the lanthanides and actinides are attributed to transitions within the 4f or 5f shell. Since the f shell lies within the filled s and p shells, it is not so strongly influenced by environmental effects and the observed transitions are sharp. They are weak, however, as transitions within the f shell are theoretically forbidden. The observed levels of the lanthanides seem to obey LS coupling, if the spin-orbit parameter Zeta is included. The ground terms of the lanthanides obey this scheme the best, but J-mixing occurs in nearly all the higher terms. LS breakdown increases rapidly until the f shell of the lanthanides is half full,

then it increases somewhat less rapidly (3). This is due not only to the fact that the spin-orbit coupling parameter is increasing faster than the electrostatic parameters, but also because the number of states having the same J-value is increasing greatly. This has the effect of increasing the "density" of these levels, thus permitting the states to J-mix more readily.

When the actinides are considered, it is seen that LS coupling is a much less reasonable choice for the calculation of energy levels. The f shell of the actinides is less shielded from the environment. Evidence has been found (3) which seems to indicate that the 5f orbitals of UF_3 in CaF_2 overlap those of the fluoride ions in the lattice. The spin-orbit coupling parameters of the actinides are about twice those of the isoelectronic lanthanides, while the electrostatic parameters are only two-thirds, so one would expect a much greater departure from LS coupling. Comparison of the ^7F term of Sm I with that of Pu I shows that while the character of this term is 95% ^7F for samarium, it is less than 50% for plutonium (3).

If LS coupling cannot be used to describe the observed energy levels of some of the lanthanides and most of the actinides, a choice must be made from other coupling schemes. Callahan's analysis of the free-ion spectrum of Gd III (18) will serve to illustrate one type of study which can be performed. Some of the low-lying configurations of divalent gadolinium appear to be $4f^7 5d$, $4f^7 6s$,

and $4f^7 6p$. The f^8 configuration is also low, but was not found in this reference. The first three configurations suggest the type of coupling known as $J_1 j$. In this scheme, the core electrons (the seven f electrons, in this case) are assumed to interact strongly with one another to form a total angular momentum, J_1. This J value then couples with the angular momentum j of the non-equivalent electron, hence the name, $J_1 j$. Although there are no restrictions on the kind of coupling assumed for the equivalent electrons, LS coupling is used in this case, mainly for simplicity. The choice, in this case, is to be made between LS and $J_1 j$ coupling, and an intermediate coupling calculation yielded the result that the $4f^7 5d$ configuration is close to LS coupling, while the $4f^7 6p$ configuration is close to $J_1 j$. An examination of the types of intermediate coupling calculations is now in order.

The basic problem, as was previously stated, is to choose which coupling scheme best fits the observed data. In order to accomplish this, a method of displaying the calculated energy levels, starting at one extreme and extending smoothly to the other, is required. When the observed levels are placed on the same scale, then the location at which the experimental and calculated levels agree most closely determines which coupling scheme is more nearly followed. The method most commonly used is to display the energy levels on a graph as a function of some parameter which indicates where the levels are located with

respect to the two coupling schemes. Dieke (2) displays intermediate coupling diagrams for the $4f^3$, $4f^{11}$, $4f^4$, and $4f^{10}$ cases. For these graphs, the energy levels are plotted for several values of the parameter, Chi, where

$$\text{Chi} = \frac{\text{Zeta}}{F_2}$$

For a particular term, the appearance of the graph is as follows: a single point is present on the plot for Chi = 0 (the case for true LS coupling) then as Zeta increases, the various J values which are characteristic of the term appear as separate points, which may or may not have separations corresponding to the Lande interval rule, depending on whether or not LS coupling is a good approximation. As was previously stated, the calculation is performed for as many values of Chi as are necessary, and the points corresponding to each J value are connected to form a smooth curve.

For this type of diagram, the transition in the type of coupling is from LS to a type called jj, where each s_i and l_i couples to form a j, and these in turn couple to form the respective J values. It is assumed that Zeta becomes very large in comparison to F_2 as jj coupling is approached, so that for this type of diagram, it is physically impossible to illustrate both extremes on the same graph. Also, it appears that the slope of some of the lines becomes quite steep as Zeta increases relative to F_2, and this might cause difficulties in determining

whether or not an experimental level corresponds to one of these lines.

Judd (27) gives expressions for the ordinate and abscissa functions of a plot which removes many of the objections to the intermediate coupling diagrams of Dieke. The first and probably most important modification is in the abscissa. Instead of plotting the levels as a function of the ratio of Zeta to the electrostatic parameter, a new function, Zi is defined, where

$$Zi = \frac{Chi}{1 + Chi}$$

and Chi = K x Zeta/G where K is a constant and G is the electrostatic parameter. In Judd's example for the sd configuration, the ordinate is obtained by solving the perturbation matrix for the eigenvalues, which are functions of Zeta and G. The function for the ordinate, Eta, is defined as

$$Eta = \frac{E - \frac{G}{4}}{(G^2 + (K \times Zeta)^2)^{\frac{1}{2}}}$$

where K = 5/2, and E is the energy level. If the Zi function is considered, first for LS coupling, where Zeta is small in comparison to G, Chi approaches zero, and so does Zi. For jj coupling, where Zeta is very large in comparison to G, then $5/2 \frac{Zeta}{G} >> 1$ and Zi approaches one. It is seen, therefore, that the transition from pure LS coupling to pure jj coupling is accomplished as Zi varies from zero to one.

For this configuration, the choice of the constants appears to arise from the functional form of the eigenvalues, in fact the expression for Eta seems to arise from the same source. In addition to the property of the Zi function, Judd lists three other characteristics of this plot. The difference between extreme Eta values is unity in the limit of G = 0 or Zeta = 0. The center of gravity of the configuration lies on the line Eta = 0, when each level has the weighting factor 2J + 1, for all values of Zi. For any value of Zi, the separations of the Eta values are proportional to the differences between the energy levels.

Callahan (18) defines Chi as Chi = $\frac{\text{Zeta}}{16G}$ and the ordinate as E/CG $(1 + \text{Chi}^2)^{\frac{1}{2}}$, where C = 5 for the $4f^7 5d$ configuration or C = 3 for the $4f^7 6p$ configuration. Recalling that the denominator of Judd's expression for Eta is $(G^2 + (K\ \text{Zeta})^2)^{\frac{1}{2}}$, if G^2 is factored out of both terms inside the parentheses, it becomes $[G^2\ (1 + \text{Chi}^2)\ ]^{\frac{1}{2}}$ or $G\ (1 + \text{Chi}^2)^{\frac{1}{2}}$, since Chi = K Zeta/G. It is seen that the denominator of Callahan's ordinate is very similar to the denominator of Judd's Eta function. The abscissa functions are the same, that is, $\frac{\text{Chi}}{1 + \text{Chi}}$, and so have the same limits, zero for Zeta = 0 and unity for G = 0. The only difference other than the numerator is that the G factor is an exchange parameter whose value is defined as being proportional to the separation between the highest levels of the two multiplets present in each configuration. Since the G value is fixed, the Zeta parameter is varied

to obtain the best fit between the observed and calculated levels. The plots of the energy levels on the intermediate coupling diagrams indicate the previously mentioned results.

Varga and Asprey (31) use an ordinate function very similar to Judd's. The expression is

$$\text{Eta} = \frac{E - \frac{F_2}{.06}}{((F_2/0.06)^2 + \text{Zeta}^2)^{\frac{1}{2}}}$$

F_2 is the first Slater integral and Zeta is the spin orbit coupling constant, both in units of wavenumbers. The factor 0.06 enables the values of Eta to be in the same range for the limits of Zeta = 0 (LS coupling) and $F_2 = 0$ (jj coupling). This expression does not retain all of the characteristics of Judd's Eta function. That is, the center of gravity of the levels does not lie at Eta = 0, nor are the extreme levels one unit apart for Zeta = 0. This does not hamper the utility of this function.

The abscissa is the same, $Zi = \frac{Chi}{1 + Chi}$, but Chi is defined as $Chi = \frac{0.06\ Zeta}{F_2}$. Using this expression, the intermediate coupling diagram for the f^2 configuration was plotted, and values of the F_k and Zeta for identification of the levels of Nd(IV) in Cs_3NdF_7 and in fluorinated borax were obtained.

For configurations with a greater number of electrons, the general complexity of the problem increases, due both to the greater number of levels which are possible and the difficulty of obtaining analytical expressions for the

levels as a function of the electrostatic parameter and the spin-orbit coupling parameter. These seem to be required if the techniques of either Judd or Dieke are to be followed rigorously. It seems, therefore, that an approach like that of Varga and Asprey is more applicable to the configurations of more than two electrons. Since the values of the highest and lowest levels are not restricted to a value of unity, this allows the levels to be spread out more, which would be important in the f^n configurations near the middle of the family.

So far, the discussion has assumed that the shell is half-full or less. When n is greater than seven, for the Nielsen and Koster tapes to work properly, Zeta must be negative. This requires that Zi be redefined, since the denominator goes to zero when Chi = -1. Varga redefined Zi in the case of negative Zetas as Zi = -Chi/(1-Chi), where Chi is still 0.06 Zeta/F_2. Note that for this expression, if Chi is a negative quantity, then both the numerator and denominator are positive, and Zi is a positive number. Chi still goes from zero for LS coupling to very large for jj coupling, so the limits of the new Zi are zero and one as before. The value of Zeta as a function of the number of f electrons increases at a greater rate than that of F_2, so a larger deviation from LS coupling is observed for the $f^{(14-n)}$ case than for the conjugate f^n case. That is, the Zi value for the f^8 case, Tb IV would be greater than Zi for the f^6 case, Eu IV.

For the LS coupling limit (Zi = 0), the Eta expression reduces to

$$\text{Eta} = \frac{0.06E}{F_2} - 1$$

Since Eta is unitless, the E values are probably a linear function of F_2, and the set of multiplet Etas will be the same for both the f^6 and f^8 configurations, and independent of the F_2 value used in the calculation. The same statement can probably be made for Wybourne's diagrams, but not for Dieke's.

If the Eta function of Varga and Asprey is considered for the jj limit ($F_2 = 0$) then the expression reduces to Eta = E/Zeta. If the energy values are adjusted by addition of a constant so that the ground state equals zero, then the energy values range from zero to $\frac{7}{2}n \times \text{Zeta}$ in steps of 1, where n = (the number of electrons for an f shell less than half full), or n = 14- (the number of electrons in an f shell which is more than half full). Therefore, the conjugate configurations f^n and f^{14-n} will have the same set of Eta values in the jj coupling limit. For the f^2 case the following results occur when the calculations are made. For $E = 0 \times \text{Zeta}$, the J-values are 0, 2, and 4. For $E = \frac{7}{2} \times \text{Zeta}$, the J-values with this energy are 1, 2, 3, 4, 5, 6. For $E = 7 \times \text{Zeta}$, the J-values with this energy are 0, 2, 4, and 6. The energy matrix for the whole configuration is block-diagonalized, with each block corresponding to one of the possible J values of the configuration,

then each sub-matrix is solved for the set of eigenvalues for that particular J. After this process is completed, the smallest eigenvalue is subtracted from all the others to yield the set of energy levels with the ground state at zero.

Now consider the conjugate configuration, f^{12}. The same set of energies, 0 Zeta, 7/2 Zeta, and 7 Zeta, will occur, but since Zeta is negative for a shell which is more than half full, the lowest energy value is now -7 Zeta and it is this term which is subtracted from all others. The effect is a rearrangement of the possible J-values for each energy level. For the f^{12} case, the following results would occur. For Eta = 0, the J-values would be 0, 2, 4, and 6. For Eta = 7/2, the J-values stay the same, 1, 2, 3, 4, 5, 6. For Eta = 7, the J-values would be 0, 2, and 4. Although the possible J-values for the Eta = 7/2 level are the same, they will not necessarily arise from the same source.

For the f^2 configuration, the ground level is the $^3H_4$ level, and, since the Eta = 0 value has one J = 4 associated with it, Varga and Asprey assign this level to that value for the jj limit. The J = 5 and J = 6 levels of this multiplet are assigned to the Eta = 7/2 level. The only other Eta value which can have a J = 6 is the Eta = 7 level, so the $^1I_6$ term is assigned to that. For the conjugate f^{12} configuration, if the J = 6 level arising from the $^3H_6$ term is assigned to the Eta = 7/2 level as it was in the f^2 case,

then the $^1I_6$ term must cross over it in order to reach the Eta = 0 level, the only other one to which a J = 6 level can be assigned. A theory by Hund (30) states that terms arising from the same configuration and having the same J do not cross as they approach the limit. Candler points out (p. 297) some experimental evidence to the contrary and indicates that Hund restricted his statement to terms which showed no symmetry property. In fact, Hund stated that if such crossing occurred experimentally, it was evidence of a symmetry property of the system. At any rate, it seems reasonable to assign the level arising from the $^3H_6$ level to the Eta = 0 value, since the $^3H_6$ level is the ground state for the LS coupling approximation. As a result of this, although the Eta = 7/2 level has a J = 6 value assigned to it for both the f^2 and f^{12} configurations, in the first case it arises from the $^3H_6$ level and in the second from the $^1I_6$ term.

For the higher configurations, the problem becomes increasingly complex, and any aid in constructing a coupling diagram, such as a table of J-values for each Eta is certainly useful. Tables have been prepared for the f^6 and f^8 configurations and will be discussed further in a later section. When the configuration contains an odd number of electrons, in the jj limit there are an even number of Eta levels, so all of the allowed J-sets will be inverted.

CHAPTER IV

TECHNIQUES OF SOLID-STATE REDUCTION

The study of naturally-occurring calcium fluoride has been of interest to researchers for more than a hundred years (6), due in part to the wide variation in colors which may occur in a single sample. The production of color in CaF_2 by radiation or additive coloration, the process of making the crystal slightly non-stoichiometric by heating in the presence of calcium vapor, has also been known for quite some time. Although methods of inducing color have been apparent for a long period of time, the interpretation of the mechanism is not yet completely resolved, since small differences and impurities in the crystals can result in widely varying results. This has resulted in a mass of papers in the literature with contradictory interpretations of the mechanism of coloration.

All of the techniques of coloration are dependent on the presence or production of defects in the crystal. In each case, the defect traps an electron or hole, creating a color center, which absorbs light. The alkaline earth fluorides apparently have no color centers such as the alkali halides, in which the F center, or electron trapped at an anion vacancy, exists (32). This reference showed

that most of the results of previously reported studies of "pure" CaF_2 were incorrectly interpreted because of the presence of yttrium in the crystals. The study reported that the presence of very low concentrations of Y(III) was enough to produce strong coloration. Only after the Y content was reduced to less than one part per million was the absorption of the irradiated crystal decreased to a low value. The mechanism of coloration of calcium fluoride must then depend on the presence of impurities. In order to understand the process by which this occurs, a discussion of the crystal structure and the effect of impurities on the structure is in order.

CaF_2 has a cubic structure of the type O_h^5, with a lattice parameter of 5.46 Angstroms. Each calcium ion is situated in the center of a cube, with a fluoride ion at each of the eight corners. Each fluoride is surrounded by a tetrahedron of calcium ions (33). The adjacent cube of fluoride ions does not contain a calcium ion, and this provides a convenient site for interstitial ions. If an aliovalent cation, a cation with a charge different from that of calcium, is substituted into the lattice at a calcium site, several types of charge compensation can be postulated. If the substituted cation has a single positive charge, the simplest type of compensation is to associate the monovalent cation with a fluoride vacany. For the trivalent case, the simplest type of compensation is the inclusion of an additional fluoride ion at the

interstitial site to account for the extra positive charge. A slightly more complex compensation mode available to the monovalent case is the association of two monovalent ions at calcium sites with a calcium interstitial. The analogous case for trivalent ions is the association of two trivalent ions at calcium sites with a calcium ion vacancy (6). These are the simplest charge compensaion models, and do not complete the list. For example, the additional positive charge of a trivalent ion can be compensated by substitution of an oxide ion for a fluoride in the lattice (34). Fong (6) cited several studies which indicated that the predominant mode of charge compensation for YF_3 and LaF_3 in alkaline earth fluorides is by interstitial fluorides. Also, a study is mentioned in which it was shown that the transference number of fluoride in CaF_2 is essentially unity and that the conductivity of CaF_2 at a given temperature was increased by the addition of YF_3 to the matrix.

The association of a trivalent impurity with its charge compensator is somewhat dependent on the concentration of the impurity. Although it is energetically more favorable to have the interstitial adjacent to the site of the trivalent ion, the difference in energy between this arrangement and one in which the interstitial is more distantly located is probably small. At low concentrations of the trivalent cation, there are many sites available to the interstitial fluoride which are not close to a

trivalent ion, but as the doping level increases, the fraction of cations which are not locally compensated becomes smaller. It has been shown (11) that as the mole percentage of holmium in CaF_2 changes from 2×10^{-3} to 3.8×10^{-1}, the percentage of total holmium reduced by gamma-irradiation goes from slightly less than 20 percent down to about three percent. Another study (35) showed that the divalent ions in the crystal were found at cubic sites. A trivalent ion which is compensated by an adjacent interstitial fluoride would have a different site symmetry. A study of Gd(III) in CaF_2 (36) reported the existence of at least eight different types of sites, depending on the method of the charge compensation of the trivalent ion. The results of these and other studies indicate that only those trivalent ions which are situated at cubic sites are capable of being reduced by ionizing radiation. If a trivalent ion is not locally compensated, the excess positive charge of the cation behaves as an efficient trap for electrons which have been freed by the ionizing radiation. However, since the non-locally-compensated ions comprise a small fraction of the total, this is an inefficient process.

Two other processes occur whereby the reduction of trivalent impurities can be achieved. Both of these methods appear to operate by the same mechanism. As was previously stated, the trivalent cations which are not locally compensated can act as electron traps, but the

fraction of ions with this property is small in normal crystals. If the compensating interstitial fluorides can be removed by some process, then the reducible fraction becomes much greater.

The first of these two processes is additive reduction, in which the doped crystal is exposed at high temperatures to vapors of the metal which makes up the cation of the lattice. A study (37) of CdF_2, which has the same structure as CaF_2 (38), showed, by exposure of a doped crystal to the vapors of Cd^{109}, that a new layer of CdF_2 is deposited on the surface of the crystal during additive coloration. The crystal was reduced with radioactive cadmium at 500 C., counted to determine its activity, then etched with a mixture of HCl, HF, and H_2O. After the surface was removed by the etchant, the count rate was redetermined and found to be negligible. It was also shown that an undoped crystal was not colored by the process of additive reduction. In this study, it was postulated that the interstitial charge compensators migrated to the surface of the crystal to react with the cadmium. At the same time, the electrons freed by oxidation of the cadmium penetrated the crystal and were captured by the dopant.

The second method involves the removal of the interstitial fluoride by migration through the crystal under the influence of an electrical field. The first study (39) showed that by application of a DC potential of 10 volts

across a 2×10^4 ohm current-limiting resistor and the crystal, reduction of about two-thirds of the samarium present in the crystal was achieved in fifteen hours. The crystal was clamped between graphite contacts in an inert atmosphere during the reduction process at 700° C. It was also stated that the rate of reduction, as estimated by the movement of induced color through the crystal, was proportional to the amount of current passed.

There are two basic differences between the crystals which are colored by radiation and those colored by electrolysis or treatment with metal vapor. The radiation-colored crystals are unstable with respect to heat and light (34). Also, the fraction of trivalent ions which can be reduced by radiation is limited, but if the charge compensators can be removed, all of the trivalent ions which are compensated by interstitial fluorides can be reduced. This is possible because, as was mentioned earlier, the fluoride ion is the dominant charge carrier in the lattice. A good comparison of the two basic processes can be found in (6). Bleaching of the radiation-reduced crystals is accompanied by fluorescence which is characteristic of the trivalent ion at a cubic site (9) when the crystal is irradiated at liquid nitrogen temperatures and slowly warmed to room temperature. In this study it is postulated that the thermo-luminescent peaks, or fluorescence which is observed as a function of temperature, are characteristic of different types of hole traps which are activated by

the increase in temperature. As the hole is freed, it migrates through the crystal until it encounters an electron trapped at a trivalent ion. Recombination of the hole and electron leave the trivalent ion in an excited state and the fluorescence is emitted during relaxation to the ground state. If oxygen is present in the crystal, bleaching by light appears to proceed in a slightly different fashion (34). This study postulates the existence of an electron trap consisting of a dysprosium ion which is compensated by an oxide ion at a fluoride site. It is stated that this arrangement is a slightly less efficient trap than the uncompensated Dy(III) ion. When the extra electron, which has been captured by the uncompensated ion, is freed, it is recaptured by the so-called RO center. This center has an absorption band slightly above 20000 cm^{-1} and the absorption at this energy is seen to increase slightly after bleaching has started. An equilibrium is established between the two sites, and both are gradually bleached after several hours. These and other studies have done much to clarify the mechanism of reduction, but other questions have been raised which will require further study.

CHAPTER V

EXPERIMENTAL METHODS

Instrumentation

The absorption measurements were made on a Cary 14 uv-visible, near-IR spectrophotometer. Spectra taken with this instrument were at both liquid nitrogen and room temperature. The infrared spectra were made on a Beckman IR-7, usually at room temperature. Two types of beam condensers were used in the infrared measurements, since the samples were small. The first was a double-lens type and the other was a four-mirror type. The latter was used for most of the spectra, since the former introduced some spurious absorption bands into the spectra. A Farrand single-beam dual monochromator spectrofluorometer with a Hanovia 150-watt xenon arc lamp was used for the fluorescence studies. This instrument has manually interchangeable slits ranging from 20 nanometer band width down to one nanometer. The output from the 1P28 photomultiplier was amplified by a RCA microammeter type WV-84C, whose output was placed across a set of variable resistors. The potential drop across this load was measured by a Texas Instrument (model PWS) recorder, which drove the scanning mechanism of the spectrofluorometer. The spectral range

of the instrument was 220 to 700 nanometers for both monochromators, and the detection monochromator was also replaced by one loaned by the Farrand Co. with a range of 700 to 1400 nanometers. A photomultiplier tube with an S-1 surface was also loaned for detection in this region. A polystyrene jacket was made for the IR-sensitive photomultiplier tube since it had to be cooled with powdered dry ice to reduce the noise level. Stanley, et. al. (40) found that for the uv-visible configuration of this same instrument, 1×10^{-6} micrograms/ml of quinine sulfate in 0.1 N H_2SO_4 was easily detectable. All samples were mounted on a cold finger by tying a fine copper wire across the face of the crystal. Thermal contact was enhanced by wetting the lower surface of the crystal with Fluorolube (grade 230, Hooker Chem. Co.). Fluorescence spectra of the crystals, before and after electrolytic reduction, were obtained at liquid nitrogen temperature. No fluorescence studies were performed on crystals reduced by gamma radiation, since after the absorption spectra were obtained, the crystals were almost completely bleached.

Electrolytic Reduction

For electrolysis of the crystals, a Hevi-duty type 70, 115 volt, clam-shell tube furnace was used to heat the crystals to the 600 to 700°C temperature range required for the electrolysis. The temperature was manually controlled by two Variacs connected to the two heating elements of the

furnace. The temperature was monitored by means of a chromel-alumel thermocouple attached to either a potentiometer or a Hoskins thermo-electric pyrometer, type HA. The reaction chamber was a 25 mm o.d. Vycor tube with a female standard taper joint on each end. The male fitting on one end contains the inlet for argon and the other fitting had openings for electrical contacts and a thermocouple well which extended to the center of the tube.

A stainless steel framework 4 cm x 1.5 cm x 1 cm with a rectangular hole 2.5 x 1.2 cm in it held the CaF_2 crystals in the furnace. A hole was drilled along the long axis at each end of the frame. One hole was five mm in diameter and was used for mechanically clamping the crystal in the framework and for electrical contact with one end of the crystal. The other was two mm in diameter and was used for electrical contact with the frame. Threaded holes for Allen screws were drilled perpendicular to each of the axial holes to hold the devices in them in place.

Several configurations of clamping and electrical contact were tried during the course of this study. The greatest single problem encountered here was thermal expansion of the framework. This caused partial or complete loss of electrical contact and, in extreme cases, the crystal fell out of the frame. The first configuration tried consisted of an alumina tube through the larger axial hole and a stainless steel wire with a tungsten tip within the tube. A loop was bent in the stainless steel

wire to compensate for the thermal expansion of the frame. This functioned as the cathode. The anode consisted of a platinum foil on the steel frame. This configuration compensated adequately for the expansion of the frame, but did not have lateral stability. In addition, the tungsten tip split some of the crystals. A more stable configuration consisted of a graphite rod through the larger hole in the frame for one electrode, and another graphite electrode electrically isolated from the frame. To compensate for expansion of the frame, a spring of molybdenum or niobium foil was used to support the insulated electrode, and another wire in an alumina tube provided its electrical contact.

Since calcium fluoride reacts with water vapor at high temperatures, all of the crystals were reduced in an atmosphere of argon. The argon was passed through a bed of copper turnings at 400°C to remove oxygen, and a drying column of anhydrous magnesium perchlorate to remove water. The gas train was composed of glass except for Tygon connectors at the joints.

The DC voltage source was a Heathkit EUW-17 transistorized power supply, and a series circuit consisting of the crystal to be reduced, a microammeter, a 10000 ohm current-limiting resistor, and the power supply was used for all the reductions. The framework containing the crystal was placed in the Vycor tube, swept with argon for a few minutes, and the temperature was slowly increased.

At about 400-450°C, the first sign of current flow was usually detected. The current generally increased with increasing temperature, but if the potential drop across the crystal was less than four or five volts, no current would flow. The minimum voltage was dependent upon the size of the crystal. Metallic dendrites, presumably calcium, always appeared either within the crystal or on the surface, and no combination of temperature or applied voltage was ever found for which reduction occurred and dendritic formation did not. The volume of the crystal in which reduction appeared to occur (as evidenced by a change in the color of the crystal) was generally confined to within one or two millimeters of the dendritic deposit. The induced color was not evenly distributed, and became darker as the deposit was approached.

Reduction by Irradiation

A Gammacell 200 (Atomic Energy of Canada, Ltd.) Co^{60} source was used for radiation reduction of the crystals. The absorption spectra from the ultra-violet cut-off to the infrared cut-off of the crystals were determined prior to irradiation. The crystals were then wrapped in aluminum foil to shut out light and for identification of each crystal. The crystals were placed in a small beaker and exposed to gamma radiation for 707 minutes. At the position occupied by the samples within the irradiation chamber, the dosage rate was calculated to be 2870 rad/min, and the

total dose was slightly more than 2×10^6 rads. After irradiation, the crystals, still in their foil wrappings, were stored under liquid nitrogen until the absorption spectra were obtained.

Absorption and Fluorescence Equipment

An all-glass, demountable Dewar vessel was constructed for the purpose of making absorption and fluorescence measurements. The inner wall of the vessel was constructed of five cm o.d. Pyrex tubing, which was necked down at the bottom to fit a three-eighths inch Kovar-to-glass seal. At the top, the inner wall was inserted through, and sealed to, the female part of a 71/60 standard taper joint. The outer wall was made from seven cm o.d. tubing, and the top was sealed directly to the male part of the standard taper fitting. A high-vacuum stopcock was attached to the outer wall to permit the assembled vessel to be evacuated. The bottom part of the outer wall was necked down and fitted with three windows, of which two were collinear, and the third was set perpendicular to the other two. The three windows were 3/4 inch diameter quartz flats, which were sealed to the body of the vessel with Glyptal. A brass fitting was machined to fit outside the Kovar-to-glass seal at the bottom of the inner vessel, so that contraction during cooling would not pull the brass away from the Kovar tube. A 13 x 13 x 2 mm brass square with a six mm hole in its center composed the lower part of the cold

finger, and the vessel was constructed so that the hole in the square was centered in the collinear windows for transmission studies. The square was set about a millimeter off the axis of rotation of the inner tube, so that by rotating it by about 45 degrees, excitation light could impinge on the sample through one of the collinear windows, and fluorescence from the sample could be observed through the perpendicular window. The overall length of the assembled vessel was 45 centimeters, and it held about half a liter of liquid nitrogen. The outside dimension of the collinear windows was 5.5 cm, and the width, measured from the front of the perpendicular window to the rearmost projection was four centimeters. The outer wall of the vessel was wrapped with black plastic tape, both to reduce stray light, and to retain fragments in case of implosion. The lower part was painted with flat black laquer to reduce stray light. After the vessel was assembled, it was found that the boiloff time of one filling of liquid nitrogen could be doubled by wrapping the inner wall with aluminum foil, since the vessel could not be silvered. This permitted one filling to last at least three hours when the vessel was evacuated with a mechanical pump. Although condensation would form on the upper portion of the vessel, none was ever observed on the windows, even on the most humid days.

For transmission studies, a 17.3 x 15.8 cm aluminum plate, $\frac{1}{4}$ in thick with a 7.5 cm diameter hole in it, was substituted for the cover of the sample compartment of the

Cary 14. Since the hole in the plate was slightly larger than the Dewar vessel, the vessel could be moved in either the x or y direction. For positioning in the z direction, a Phenolic clamp was fastened around the outside of the vessel, so that the lower part of the clamp was 8.5 cm above the center of the 6 mm hole in the cold finger, which centered it in the light path of the Cary 14. The clamp was wide enough to completely cover the hole in the aluminum plate, so the sample compartment was light-tight for all positions of the Dewar.

The samples were fastened over the 6 mm hole in the brass plate. Since they did not always completely cover the hole, copper foil with a hole in it conforming to the shape of the sample was wrapped over the brass plate to insure that all the light reaching the detector passed through the crystal. The samples were tied to the plate-foil arrangement with fine copper wire and thermal contact was enhanced with Fluorolube oil, in much the same fashion as for the fluorescence studies. If the crystal to be studied was not too large, the Fluorolube alone was found to be sufficient to hold the sample in place, provided the Dewar could be maintained in a semi-horizontal position until the sample cooled down enough for the Fluorolube to thicken.

The combination of the four surfaces of the quartz flats, the 6 mm hole in the cold finger (the size of the light beam in the Cary 14 is about one cm), and the low

transmittance of the reduced samples produced large absorbance readings on the Cary 14. To alleviate this, a set of six masks for the reference beam were made from copper foil. Using these masks, the apparent absorbance of the sample could be reduced from 0.45 to 1.8 absorbance units, depending on which mask was used. The masks consisted of a piece of foil 1 x 5 cm, with rectangular holes, whose length was 0.5 cm and perpendicular to the long dimension of the strip. The width of the hole determined the absorbance of the strip. All the holes were centered 1.3 cm above the bottom end of the strip. The masks did not affect the flatness of the baseline except for a small region near 350 nanometers and at the maximum wave lengths. Of course, the masks widened the slits of the monochromator, but not to an unreasonable degree, and they permitted the absorption spectra of many samples to be determined without cleaving or grinding down and repolishing the crystals.

Materials

CaF_2 single crystal chips were obtained from Semi-elements, Inc. (Saxonburg, Pa.). The nominal concentration of crystals doped with Pr, Gd, Ho and Er was 0.1 mole percent. The same value for the Ce-doped crystal was 0.25 mole percent. The crystals were grown from the anhydrous rare earth fluorides and calcium fluoride by the Bridgeman technique under vacuum (41).

CHAPTER VI

EXPERIMENTAL RESULTS

Absorption and Fluorescence Spectra

The absorption spectra of samples were determined both before and after reduction by both techniques. The fluorescence spectra of the samples which were electrolytically reduced were determined in the same fashion. The radiation-reduced samples bleached out so rapidly during the determination of their absorption spectra that no attempt was made to obtain fluorescence spectra, so any time fluorescence is discussed, it will be on either the oxidized form of the lanthanide, or an electrolytically reduced sample.

Cerium

The cerium-containing samples were tannish-brown in color, very brittle and difficult to cleave without shattering the crystals, and appeared to contain some sort of inclusions when examined under a microscope. The crystals were unstable to heat and crumbled if subjected to much pressure. Also, when a crystal was heated to 400-500°C in argon and then returned to room temperature, the appearance was changed drastically. After heating, the crystals were

gray in color, and microscopic examination showed the presence of black particles similar to the previously mentioned inclusions, only much larger in size. Electrolysis attempts were generally unsuccessful, due either to shattering of the crystal or loss of electrical contact. One sample appeared to conduct current for awhile, but no change in color of the crystal was observed, other than that due to heating. The unreduced crystals displayed a gradually increasing absorption in the visible region, probably due mainly to scattering, but low peaks at 17000, 19500, 22000, 25800 and 27400 wavenumbers were observed. In the ultraviolet region a very intense peak, centered at about 31000 wavenumbers was observed, the maximum of which could only be observed on the thinnest samples. The transition from the ground state of the f^1 configuration to the $^7F_{7/2}$ level at about 2200 wavenumbers was not observed in absorption.

A peak centered at about 32440 cm^{-1} was observed in praseodymium samples. The total width of the peak was about 1200 cm^{-1}, and it was rather broad with indications of several weak shoulders on it. The lowest portion of the peak contained a very sharp and prominent shoulder at 31950 cm^{-1}, and there was the indication of at least three weak shoulders between it and the central peak. On the high-energy side of the central peak, there were indications of at least three more weak shoulders. The interval between the strong peaks was 490 cm^{-1} and the intervals

between the two shoulders and the central peak were about 80 and 90 cm^{-1}. The locations of the high-energy shoulders were difficult to determine, but the intervals seemed to range from 150 to 170 cm^{-1}. The weakest shoulder on the low-energy side had an interval between it and the sharp peak of about 180 cm^{-1}.

It has been reported (25) that the first f-d transition of trivalent cerium in CaF_2 occurs at 32400 cm^{-1} and exhibits vibronic structure. Two types of structure occur; a major interval of 460 cm^{-1} and a minor interval of 150-180 cm^{-1}. The major peaks were reported to occur at 31940, 32400, and 32860 cm^{-1}. The correspondence in energy between the first two of these peaks and the peaks observed in the praseodymium crystals, as well as the intervals of the shoulders, is so strong that it must be concluded cerium in the trivalent state occurred in very low concentrations as an impurity in the praseodymium crystals.

The irradiated cerium-containing crystal exhibited a very intense, broad absorption band with the maximum at 19900 cm^{-1} and shoulders at 10300, 12300, 15700, and 22000 cm^{-1}. There was no evidence of absorption below the first shoulder mentioned, in agreement with previously reported spectra (8). No fluorescence was observed for the crystals, either before or after reduction.

While the presence of the strong band at 32000 wavenumbers indicated that there was some trivalent cerium present in the crystals, the absorption bands present in

the visible would seem to indicate the presence of either cerium in some other form, such as CeO_2, which is reddish, or some other undetected impurity. Studies of trivalent cerium in CaF_2 (25, 42) make no mention of any absorption bands in the visible region.

Praseodymium

In the absorption spectra, all of the predicted levels of trivalent praseodymium above 4000 cm^{-1}, except the $^1S_0$ level, were observed during examination of the samples prior to reduction. Omitting the $^1S_0$ and the $^3H_5$ levels from the list, the remaining 11 levels were least-squares fit with six parameters with a root-mean-square deviation of 61.7 wavenumbers. F_2 was found to be 306.0 cm^{-1} and Zeta was 750.9 cm^{-1}, compared to 305.4 cm^{-1} and 730 cm^{-1} from reference 31. Fluorescence from the ^3P multiplet and the $^1D_2$ level to the ground state was observed during examination of the samples by this method. No impurities other than the Ce(III) were detected.

The reduced samples agreed with previously published spectra (8), with bands at 4000, 8600 and a low, wide band centered at 15000 cm^{-1}. In the visible region, more intense bands were observed at 20000, 22300 and 25500 cm^{-1}. It is interesting to note the correlation between these three bands in the visible and the three central bands mentioned in the section on trivalent cerium. While it is difficult to draw any conclusions about impurities from

such limited information, it is within the realm of possibility that the cerium crystals were contaminated with praseodymium, thus accounting for the coloration of the cerium-containing crystals in the visible region. No fluorescence was observed in the reduced samples which could not be attributed to that from the trivalent ions.

Gadolinium

The absorption spectra of the gadolinium-containing unreduced crystals exhibited no absorption except for the weak lines due to the ^6P multiplet. This was also seen in fluorescence. In addition to this fluorescence transition, one other was observed at about 15900 cm^{-1} and was believed to be due to trivalent europium, probably the $^5D_o \rightarrow {}^7F_2$ transition.

When the samples were electrolytically reduced, the initial color of the reduced region was a reddish-blue. After a few days, the edges of the colored region appeared to be pink, but after the color finally stabilized to blue-green, no evidence of the initial red color was seen. The only obvious change in the absorption spectra during this period was an enhancement of a band at 25500 cm^{-1} and a shift of the 17300 cm^{-1} peak to about 18000. All these bands were at least 3000 wavenumbers wide, and it was not always possible to position the sample in the light path of the Cary 14 at the same place, so it was difficult to tell if the observed shifts were due to a change in the spectra,

or merely due to an examination of a different region of the crystal. After the color of the reduced crystal had stabilized, the observed spectrum agreed with the published one (8), with peaks at 18000, 25500, and 31000 cm^{-1}, but an additional one at 35800 cm^{-1}.

The radiation-reduced crystal had a color similar to that of the electrolytically reduced crystal immediately after reduction. That is, it was a bluish-purple color, and the positions of the absorption bands differed only slightly, being found at 18400, 25000, and 31000 cm^{-1}. The band with a maximum at 18400 was more intense than the other two, and had a shoulder at 17500 cm^{-1}. There was also a very weak indication of a band centered at 12000 cm^{-1}. No changes in the apparent color of this crystal during the absorption measurements were observed, but after being stored in a tape-wrapped desiccator for about three months, it was unwrapped from aluminum foil, it was found to have changed to a light green color, similar to that of praseodymium in borax. While the crystal was being mounted in the cold finger, the color changed back to the original bluish-purple. The change must have been due to the influence of the fluorescent lights in the laboratory. No explanation for this behavior can be given.

The fluorescence of the electrolytically reduced crystal was first incorrectly thought to be at about 1.3 micrometers, or 7100 wavenumbers, but this could not be explained in terms of either the f^8 configuration or the

f^7d configuration, because of the absence of levels in this region which might fluoresce. It was then recalled that the monochromators used in the spectrofluorometer yielded strong second order radiation, so a search was made at half the apparent wave length and a weak peak at 665 nanometers, or 15000 wavenumbers was observed.

Since the presence of impurities in the crystals had already been observed, a study of the literature was made to determine if this level could be ascribed to either europium or terbium. The fluorescence of europium usually occurs from either the $^5D_0$ or $^5D_1$ levels, and laser emission has been observed (4) for the $^5D_0 \rightarrow {}^7F_2$ transition in the region of 16300 cm^{-1}, and this transition is apparently a strong one in a number of host lattices and compounds. The cubic crystal field analysis for trivalent terbium in CaF_2 has been reported (26), and the fluorescence from the $^5D_4$ level to the $^7F_5$ level of the ground multiplet should occur in the region of 18400 cm^{-1}. The absorption and fluorescence spectra of Sm(II) in CaF_2 have been reported (24), and the highest energy line appears at 14497 cm^{-1}. The most intense line appears at 14114 cm^{-1}, or about 708 nanometers. The error in calibration of the detection monochromator was probably no more than four nanometers, so it is unlikely that the observed line is due to samarium. It has been reported (2) that divalent samarium is a persistent impurity in some crystals, and is detectable in very highly purified salts.

While the presence of other unidentified impurities as the source of the fluorescence could not be ruled out, the assumption was made that the fluorescence was due to a transition from the $^5D_4$ level of the f^8 configuration to either the J = 4 or J = 5 level of the ground state ^7F multiplet. The calculations based on this assumption will be described in a later section.

Holmium

The holmium-containing crystals were examined in absorption prior to reduction, and it seemed that they contained less of the dopant than some of the other crystals, since the observed f-f transitions were weaker than in other crystals. After electrolytic reduction, the crystals were re-examined, and the observed spectra corresponded to those previously published (35), with bands centered at about 11000, 14600, and 19300 cm^{-1}. They were, however, much weaker.

One of the crystals which had been partially electrolytically reduced was included with the batch of crystals which were irradiated. The crystal was darkened at the cathode end, where the metallic dendrites were, but at the other end of the crystal, which had been the anode during the electrolysis, no coloration was observed. As was previously stated, the trivalent ions, at the site occupied by a divalent ion in the lattice, act as electron traps unless the excess positive charge is compensated for

by a nearby interstitial anion. When a potential is applied across the crystal, the interstitial anions migrate toward the anode, creating more uncompensated trivalent ions at the cathode end, and reducing the number of uncompensated trivalent ions at the anode end of the crystal. Since there were fewer uncompensated lanthanide ions at the anode end, the amount of coloration induced by the radiation at that end was lower.

In addition to the previously reported peaks, others at 22500, 27800, 32000, 39500 and 43000 cm^{-1} were observed. The first of these is also reported in reference eight. The fact that the crystals used in this study were so dilute in holmium accounts for the additional lines, since the other reports indicated that the absorbance became too high to measure at about 25-27000 cm^{-1}. No fluorescence lines were observed in the reduced crystals which could not be accounted for by that of the trivalent ion.

Erbium

When a section of the erbium-containing crystal was electrolytically reduced, for two or three days after the process was completed, the only color change observed was a reddish-orange color in the region near the metallic dendrites, similar to that observed in most of the crystals containing other lanthanides. After this period, a greenish region appeared, which extended one or two millimeters beyond the orange area. This region reproduced the

previously reported (8) peaks at 10400, 16500, 20200, and 25800 cm^{-1}. In addition to these, the irradiated sample exhibited absorption peaks at 29200 and 32600 cm^{-1}. No fluorescence not attributable to the trivalent ion was observed.

Free-ion Levels from Spectroscopic Data

Cerium III ($4f^2$)

Sugar (14) published an extension on the line list of divalent cerium. In this paper, ten of the 13 possible lines of the f^2 configuration were identified, the only omissions being the ^3P multiplet. The first two columns of Table I give the experimental values and Russell-Saunders labels from (14). The third column gives the deviation of the calculated values from the observed levels. The fourth column gives the final values of the Racah parameters and the root-mean-square deviation. On initial runs of the program, the experimental values for the $^1S_0$ and $^1I_6$ levels were included in the data set, but they degraded the fit to the lower levels, so they were omitted in the final calculation. This effect was also noted in calculations performed on Pr(III), where the program consistently placed the $^1I_6$ level below the $^3P_1$ level, whereas studies for several crystals systems have shown it to be above (2). The values of F_2 and Zeta of this configuration are 235.35 and 544.25, respectively.

TABLE I

Ce III CALCULATION

LS Name	J	Eobs	Ecalc-Eobs	
^3H	4	0.00	0.0	E_0 = 5034.90
	5	1526.36	1.10	E_1 = 3481.13
	6	3127.05	- 2.13	E_2 = 17.13
^3F	2	3762.71	-11.77	E_3 = 359.47
	3	4764.76	- 1.99	Zeta = 544.25
	4	5006.06	6.66	RMS = 8.52
^1G	4	7120.00	-10.43	
^1D	2	12835.70	0.12	
^1I	6	17420.60		
^1S	0	32838.62		

Praseodymium III (f^3)

The spectroscopic data on this configuration were obtained by Sugar (43) and analyzed by Trees (15). In these papers, 38 out of 41 possible levels of the f^3 configuration were identified by the authors. Using these values for the energy levels, a number of combinations of the variable parameters and sets of the energy levels were put into the program. As it was originally written, it could only accept 20 energy levels, so some of the lowest levels for each J-value except $J = 17/2$ were used in the computation. The three lowest levels for the $J = 3/2$, $5/2$, $7/2$, $9/2$, and $11/2$; the two levels given for $J = 1/2$ and two of the three levels for $J = 13/2$; and one of three levels for $J = 15/2$ were fitted with four parameters and yielded a rms deviation of 236 cm^{-1}. With six parameters the deviation was reduced to 192 cm^{-1}. The proper arrays in the program were then redimensioned to allow for up to 40 levels, and several runs were made with either 38 or 37 levels and six variable parameters. After three trials, the rms deviation was still decreasing, but so slowly that no further calculations were performed. The final result was an F_2 of 280.6 cm^{-1} and a Zeta of 664.9 cm^{-1}.

Holmium III (f^{11})

A list of six lines identified as belonging to the f^{11} configuration of divalent holmium has been published (17).

These included the ^4I multiplet including the ground state of J = 15/2, the $^4F_{9/2}$ level, and the $^2H_{11/12}$ level. Although these were only a few of the 41 possible levels, the calculation was performed to obtain values of F_2 and Zeta for Figures 1 and 2 and to compare with those given in another paper (35) for Ho(II) in CaF_2. F_2 and Zeta values of 395 cm^{-1} and -2008 cm^{-1}, respectively, were obtained compared to about 400 cm^{-1} and -1982 cm^{-1} from the second reference.

Additional Information

In the section in Dieke's book (2) on divalent rare earths in crystals, a diagram of levels attributed to Sm(II) in $LaCl_3$ was shown, along with the same levels of trivalent europium (f^6) calculated with F_2 and Zeta reduced by 20% and 22.2%, respectively. Using the values for Eu(III) from page 65, the reduced values for F_2 and Zeta were 321 cm^{-1} and 1027 cm^{-1}, respectively. The values of Zeta for Tm III (f^{13}) and La III (f^1) can be found in references 8 and 13. All these values are compiled in graphic form in Figures 1 and 2, along with the corresponding values for the trivalent ions.

Divalent Gadolinium

The absorption spectrum of divalent gadolinium observed in this study, for both the gamma-reduced and the electrolytically reduced crystals, agreed with the

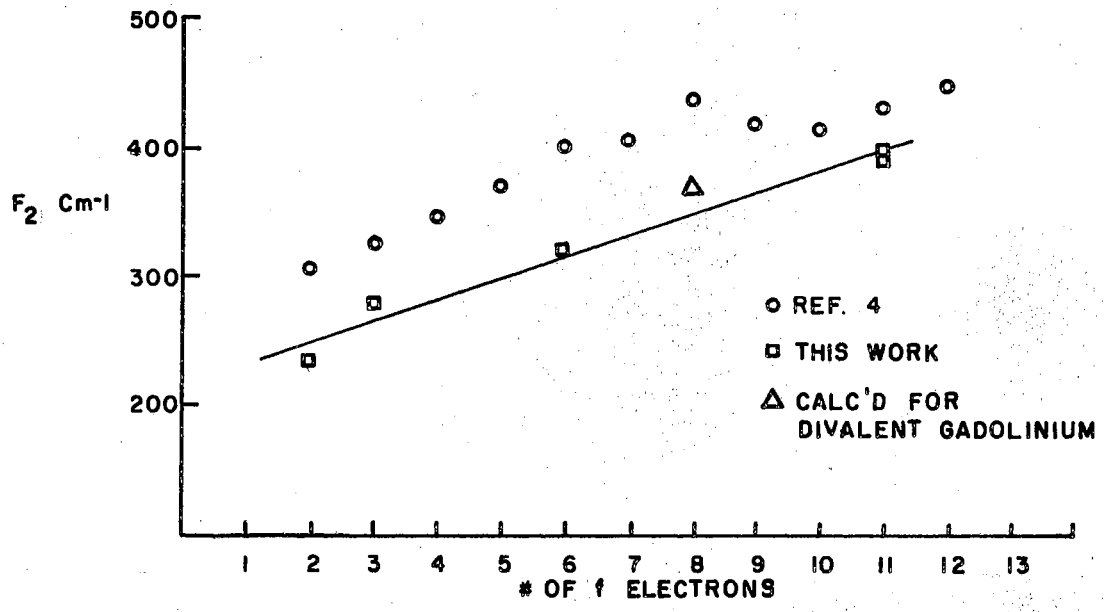

Figure 1. F_2 Versus the Number of f Electrons

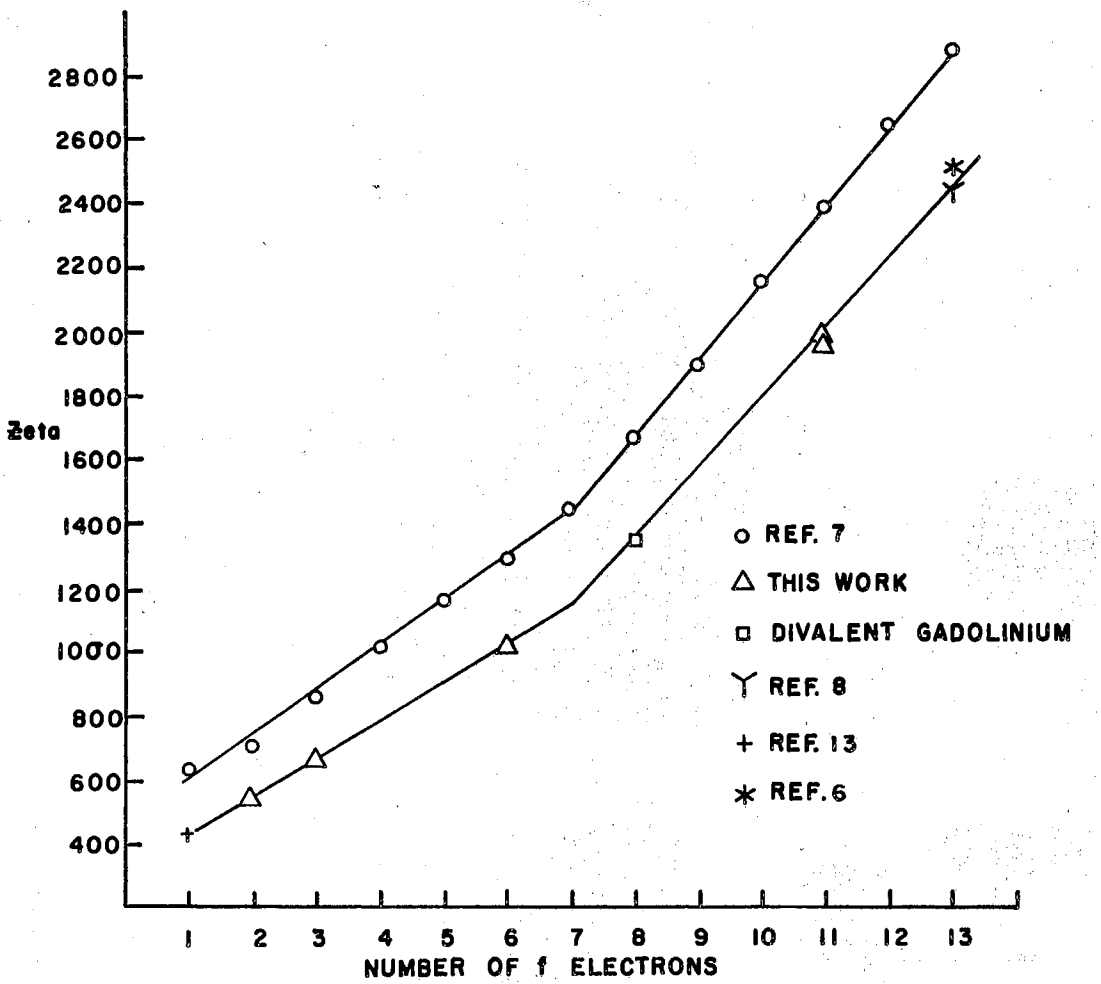

Figure 2. Zeta Versus the Number of f Electrons

published spectra (8). The fluorescence spectrum of the electrolytically reduced crystals, however, exhibited a very weak fluorescence centered at about 15000 cm^{-1}. This did not appear to be due to any impurity, so under the assumption that it was due to a transition from the $^5D_4$ level to the $^7F_4$ or $^7F_5$ level, values of F_2 and Zeta were sought to reproduce the energy difference between the $^5D_4$ level and the average of the $^7F_4$ and $^7F_5$ levels. Figure 2 had been plotted for the trivalent ions and the Zeta values for the divalent ions seemed to parallel the two halves of the trivalent part of the figure. Therefore, a straight line was constructed through the Zeta values from one to six electrons, and this line was extended to intersect with the f^6 line of the ordinate. By fixing the start of the second half of the divalent figure at this point, another straight line was constructed through the points for divalent holmium and thulium. This fixed the value for Zeta at -1360 cm^{-1}. A series of calculations were then performed by varying F_2 until the energy difference between the two levels was 15000 cm^{-1}. During this process, it was noted that the positions of the levels of the ^7F multiplet were virtually unaffected by changes in F_2, indicating Russell-Saunders coupling is a good approximation for this relative method of calculation. The initial guess for F_2 in the calculations was obtained from consideration of Figure 1. Values of F_2 for Ce III (f^2), Pr III (f^3), Sm III (f^6) and Ho III (f^{11}) had been plotted on Figure 1,

so a straight line was constructed through these points and the intersection for the f^8 case was used in the first calculation. After a couple of trials, it was noted that the difference between the two levels, divided by the position of the higher level was about equal to the difference in the two values of F_2, divided by the larger, so this information was used to compute the final value of F_2, 371 cm^{-1}.

The Intermediate Coupling Calculations for the f^6 and f^8 Configurations

It should be borne in mind that many approximations are built into calculations of this type. It has been assumed that higher configurations of the ion do not interact with the one under consideration, but there is much experimental evidence to the contrary (3). A second assumption is that the ratios of the Slater integrals for the 4f shell of the lanthanides are the same as for the 4f shell of hydrogen, for which the ratios may be calculated exactly. Another approximation is that the electrostatic interactions described by the Slater integrals or the Racah parameters and the magnetic interaction described by the spin-orbit coupling parameter are the only ones which must be considered in a description of the behavior of the energy states of a partially-filled f shell. The degree to which these and other approximations made during the course of an intermediate coupling calculations

are valid depends to a large extent on the accuracy required of the result. In other words, if it is desired to fit a set of levels precisely, more parameters must be included in the calculation in order to achieve the required agreement, but if the study of the set of levels is only a preliminary one, then the approximations made are sufficient.

In this study, the expression

$$Eta = \frac{E - \frac{F_2}{.06}}{((F_2/0.06)^2 + Zeta^2)^{\frac{1}{2}}}$$

was used for the ordinate for both the f^6 and f^8 configurations. The expression $Zi = \frac{Chi}{1 + Chi}$ where $Chi = 0.06\ Zeta/F_2$ was used for the f^6 configuration and

$$Zi = \frac{-Chi}{1 - Chi}$$

was used for the f^8 configuration, with Chi defined the same as before. 4f hydrogenic ratios of the F_k were assumed in the calculations performed for this study. Table II lists the values of F_2, Zeta, and Zi which were used for the ordinates of the f^6 and f^8 intermediate coupling diagrams, with the units of F_2 and Zeta in wavenumbers.

For the f^6 configuration, the Zi values of 0.160 and 0.165 correspond to the F_2 and Zeta values given by Ofelt (44) for divalent samarium and trivalent europium, respectively. The fact that these values for divalent

TABLE II

F_2, ZETA, AND Zi VALUES

f^6 Configuration			f^8 Configuration		
F_2	Zeta	Zi	F_2	Zeta	Zi
400.0	1×10^{-6}	0.0	400	- 740.7	0.1
400.0	740.7	0.1	371.0	-1360	0.18
330.0	1050.	0.160	434.0	-1705	0.191
401.0	1320.0	0.165	465.8	-2270.	0.226
300.0	2692.3	0.35	300.0	-2692.3	0.35
200.0	3333.3	0.50	200.0	-3333.3	0.5
100.0	5000.	0.75	100.0	-5000.	0.75
0.0	1×10^{4}	1.0	0.0	-1×10^{4}	1.0

samarium are slightly different from those cited previously makes a difference of only one unit in the third decimal place of Zi, and it was concluded that this was of no consequence. The rest of the values of F_2 and Zeta were obtained by selection of regularly spaced values of Zi. The expression for Zi was then solved for the ratio of Zeta to F_2, decreasing values of F_2 were chosen and the corresponding value of Zeta was calculated. The value of F_2 at the LS coupling limit was chosen at 400 cm^{-1} because both the value for F_2 for europium and terbium in the trivalent state are in this range.

The Zi values listed in Table II for the f^8 configuration, of 0.18, 0.191, and 0.226 correspond to the F_2 and Zeta values calculated in this work for divalent gadolinium, Ofelt's values for trivalent terbium, and the parameters which describe tetravalent dysprosium from Varga and Asprey (20), respectively. The other values were obtained as previously described. Calculations for the LS coupling limit were not performed for the f^8 case, since the results would have been identical to that for the f^6 configuration. It was only after Tables III and IV were constructed as an aid in completion of the diagram that the symmetry of the number of J-values in each Eta level for the two configurations was found.

The two tables were constructed by inspection of the computer output of the two configurations for the limiting jj case. The Eta values are listed on the first row of

TABLE III

f^6 CONFIGURATION, ALLOWED J VALUES FOR EACH ETA

J Values	Eta Values						
	0	3.5	7	10.5	14	17.5	21
0	1		3	3	5	1	1
1		1	2	8	5	3	
2		1	7	11	13	4	1
3		1	5	15	11	5	
4		1	8	15	16	5	1
5		1	5	14	12	5	
6		1	6	13	13	4	1
7			3	10	8	3	
8			3	7	8	2	
9			1	5	4	1	
10			1	3	3	1	
11				1	1		
12				1	1		
Total No. of Levels	1	6	44	106	100	34	4

TABLE IV

f^8 CONFIGURATION, ALLOWED J VALUES FOR EACH ETA

J Values	Eta Values							
	0	3.5	7	10.5	14	17.5	21	Rank
0	1	1	5	3	3		1	14
1		3	5	8	2	1		19
2	1	4	13	11	7	1		37
3		5	11	15	5	1		37
4	1	5	16	15	8	1		46
5		5	12	14	5	1		37
6	1	4	13	13	6	1		38
7		3	8	10	3			24
8		2	8	7	3			20
9		1	4	5	1			11
10		1	3	3	1			10
11			1	1				2
12			1	1				2
Total No. of Levels	4	34	100	106	44	6	1	295

each table and the J values are given in the first column on the left. The column on the right of the f^8 configuration, in Table IV, gives the rank of each J matrix, and 295 is the total number of levels of all J's. For an Eta value of seven in the f^8 configuration, there are 16 levels which terminate here with a J value of four. Blank spaces in a column indicate that for that Eta value, there are no levels of a particular J which terminate there. The bottom row gives the total number of levels of all J values which terminate at that Eta value.

Brief inspection of the tables indicates the previously mentioned symmetry. When the totals are considered, it is also obvious that all of these levels could not be plotted on a single diagram. In fact, for some of the J-values, a plot containing all of the J's terminating in a particular Eta would probably be unwieldy. It was therefore determined that the diagrams should be drawn for each LS term, with an effort made to keep each multiplet on the same scale, so that they could be reproduced and combined if desired. The scale of the original drawings was one inch per Eta unit on the ordinate. When they were reduced for printing, an effort was made to have all of them reduced by the same amount, so that they would remain on the same scale. It is suggested that if a composite of several multiplets is desired, they either be separately Xeroxed onto transparencies and overlaid, or that they be traced off onto a single page. If the multiplets are Xeroxed onto

transparencies, it is suggested that the abscissa be masked off if possible, since the scale on the bottom and the legend tend to add to the confusion.

Since only the lower multiplets were considered, a choice had to be made as to where to stop. All the Eta values for the LS limit were plotted and a pair of multiplets, which the program denoted as ^5F and ^5I lay just below 40000 wavenumbers, and the density of terms was low in this region, so it was decided that these two multiplets would be the highest ones considered.

Although essentially no faith can be put in the numerical values of the energy levels of the highest terms in the two conjugate configurations, the degree to which they are incorrect will probably not vary too much between the terms, so their relative spacings might be fairly correct.

Many lines observed in free-ion spectral studies arise from transitions between different configurations of the same ionization state. The parity of a configuration is defined as the sum of the one-electron orbital angular momenta of the configuration (3). If the sum over the electrons is odd, the configuration is said to be of odd parity, and is called an odd configuration. An atom or ion in an excited state can make a transition to a lower configuration of opposite parity with emission of a photon. Likewise, the transition from a lower configuration to a higher one of opposite parity by absorption of energy is also allowed. If the energy separation between the two

configurations is of the right order of magnitude, then the emission lines will be accessable to the spectroscopist. Since the highest levels of the f^6 and f^8 configurations are more widely spaced than a lot of other levels, and thus more easily recognizable, a figure describing the variation of the levels with the change from Russell-Saunders to jj coupling was included. The scale for this diagram is one inch per 0.2 Zi units, and one inch per two Eta units.

For the f^6 configuration, the Eta = 0 value could only accept one level with a J-value of zero, so this was easily assigned. The Eta = 3.5 value could accept a total of six J-values, so these, too, were easily assigned. Thirty out of the forty-four possible J-values were assigned to the Eta = 7 value. On the diagram for the high terms, the four possible J-values of the Eta = 21 were assigned, seven of the thirty-four possible J-values were assigned for the Eta = 17.5 level, and a single J = 0 level was indicated as heading toward the Eta = 14 value which was not shown on the diagram.

Since the Eta = 21 level of the f^8 configuration had only one J = 0 term, it was satisfied, although not without difficulty. All six of the levels terminating at Eta = 17.5, and the five remaining levels were indicated as going to Eta = 14. To summarize, 49 of the 295 levels were assigned. The theory of Hund which was previously cited was generally followed with no difficulty for the lower diagrams, but seemed to be freely violated for the highest terms. The

details of the individual figures will now be considered.

The f^6 Diagrams

The levels of J = 0, 1, 2, 3, 4, 5, and 6 originating in the ^7F multiplet (Figure 3) were assigned in the jj limit to the Eta values of 0 and 3.5, with the single J = 0 term going to the Eta = 0 level and the rest terminating at Eta = 3.5. The multiplet remained erect except for the J = 6 level, which is just above the J = 2 level when Zi = .75.

The calculated or experimental Eta values were not plotted on the figures in order to keep them uncluttered. As an illustration of the type of results which can be obtained from these figures, and as an example that the usefulness of the figures is not restricted to the lanthanides, two cases for the actinides will be considered. F_2 and Zeta values have been reported in the literature for a few low levels of Am IV and Pu I (37). The ^7F multiplet, the $^5L_6$ level, the $^5D_2$ level, and the $^5G_2$ level were used in obtaining the F_2 and Zeta values for Am IV, which has the $5f^6$ configuration. For Pu I, which has the $5f^6 7s^2$ configuration, only the energy levels of the ^7F multiplet were reported. The two electrons in the 7s shell do not interfere significantly, since they constitute a closed shell. Using the values $F_2 = 268.6$ cm^{-1} and Zeta = 2605 cm^{-1} for Am IV, experimental Eta values were calculated and compared to the graphical Eta values at Zi = 0.368. If the root mean square of the Etas is

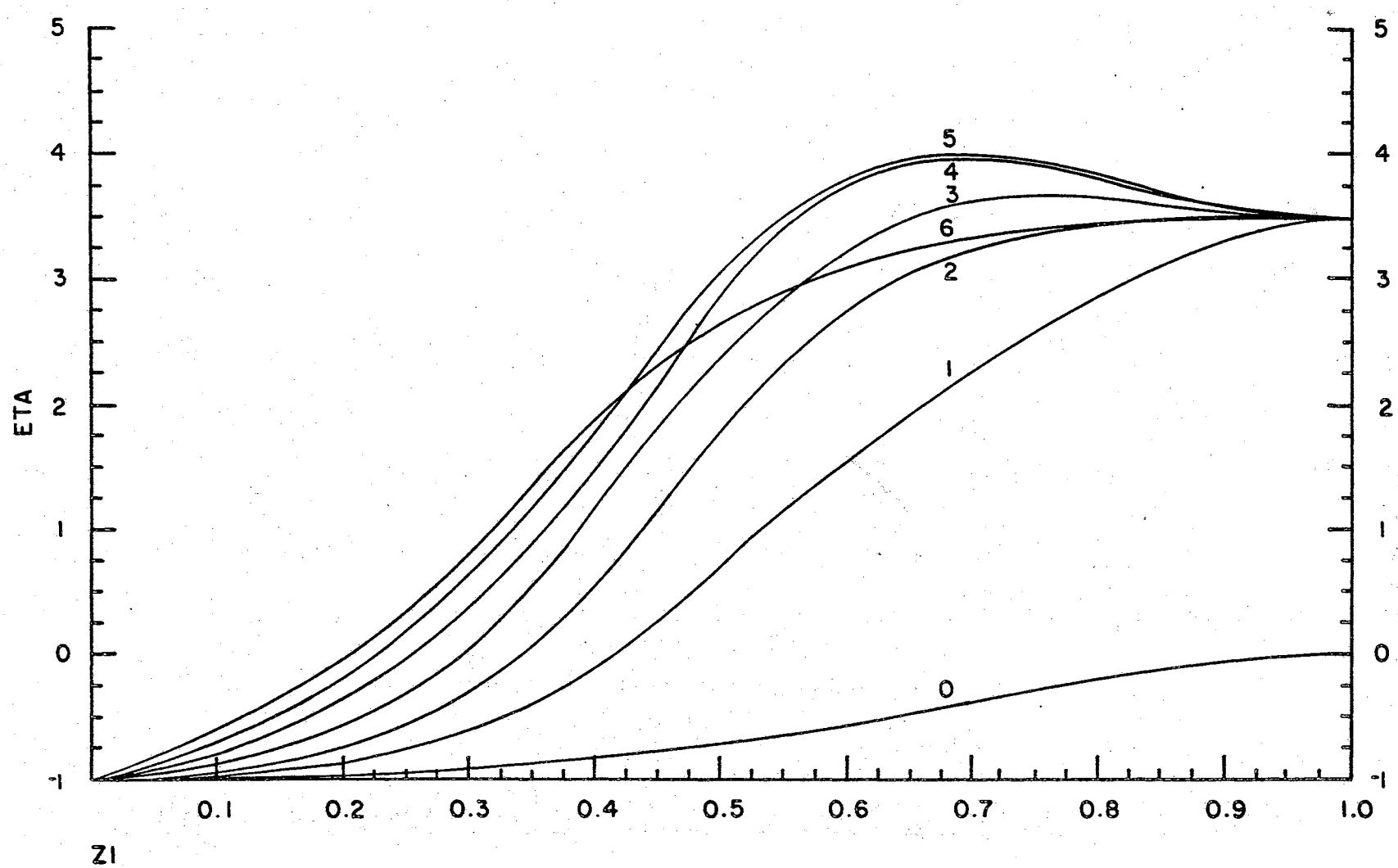

Figure 3. ^{7}F Term, f^{6} Configuration

calculated from the expression

$$\text{rms Eta} = (\Sigma(\Delta)^2 / (n-1))^{\frac{1}{2}},$$

where Δ is the difference between the corresponding experimental and graphical Eta values and n is the number of levels, then for Am IV the rms Eta value was 0.106. The agreement was considered satisfactory, since the range of Etas spanned nearly 4.25 units and three of the levels accounted for almost 75% of the error. For Pu I, the values of F_2 and Zeta of 230.6 cm^{-1} and 2174.6 cm^{-1}, respectively, yielded a set of Etas which, when compared to Figure 3 at Zi = 0.361, had a rms Eta of 0.064 for a range of 2.2 units. At this point, the J = 3 level contributed almost two-thirds of the total error.

Figure 4 gives the behavior of the J = 0, 1, 2, 3, and 4 levels arising from the ^5D term. The multiplet is erect for the LS approximation, and remains so, except for the J = 1 level, which becomes the highest in the limit of jj coupling. The experimental Eta of the J = 2 term for Am IV was within 0.08 units of the graphical value. A value of 9772.5 cm^{-1} has been reported (46) for the $^5D_0$ level of Pu I, placing it 466 cm^{-1} below the J = 6 level of the ^7F term. On Figure 4, this level would be about 0.157 Eta units below the graphical value, still within a reasonable range for identification purposes, since it is the only J = 0 level in that region of Eta values. It is interesting to note that a composite of Figures 3 and 4 indicates that

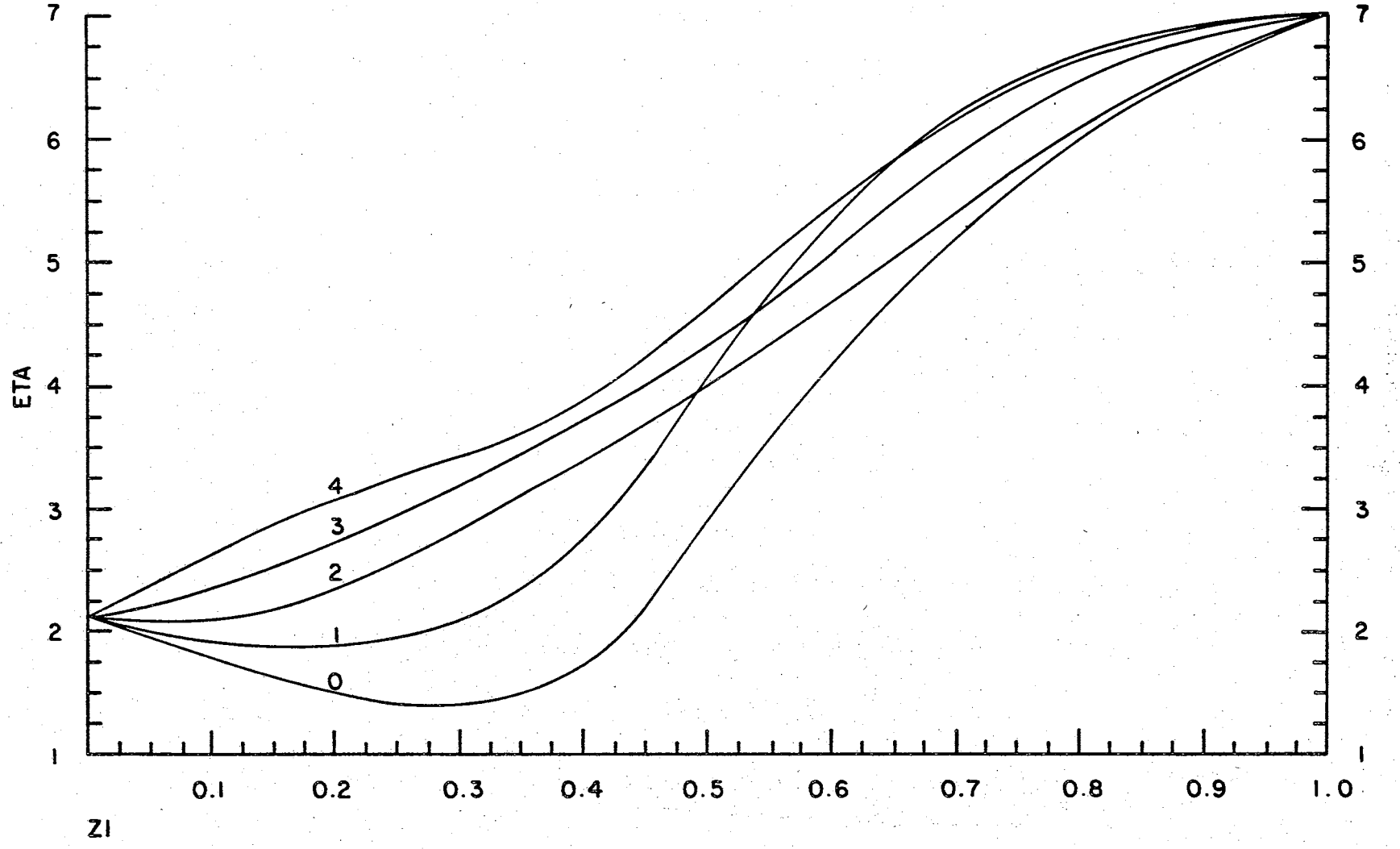

Figure 4. ^5D Term, f^6 Configuration

the J = 0 level lies below the J = 6 level for Zi values from 0.370 to 0.465, although it has been reported (3) that no set of F_2 and Zeta values will yield this result if the 5f hydrogenic ratios are assumed. In short, although the order of the two levels is not predicted correctly for the Zi value of Pu I, the crossover point is close by, and is probably a function of the drawing of the figure.

The ^5L term gives rise to J values of 6, 7, 8, 9, and 10, all of which terminate at Eta = 7 (Figure 5). All the levels remain erect except for J = 10, which is below J = 8 in the jj limit. The J = 6 experimental Eta lies nearly 0.2 units above the graphical value and is the largest contributor to the error in the calculation for Am IV. During the calculations for these diagrams, the two lowest J = 6 values seemed to approach one another, but it was decided that they should not cross, and that the lower should terminate at Eta = 3.5. It is felt that these two experimental points justify the choice, since, if the alternate option had been taken, the result would have been a larger deviation from the experimental Etas of both the terms. That is, crossing the two J = 6 levels would have lowered the graphical value for the level arising from the ^5L term, and it was already too low, while the ^7F level would have been raised from a position which is greater than the experimental Eta to one at least a tenth of a unit higher.

Figure 6 indicates the assignments of the J = 2, 3, 4,

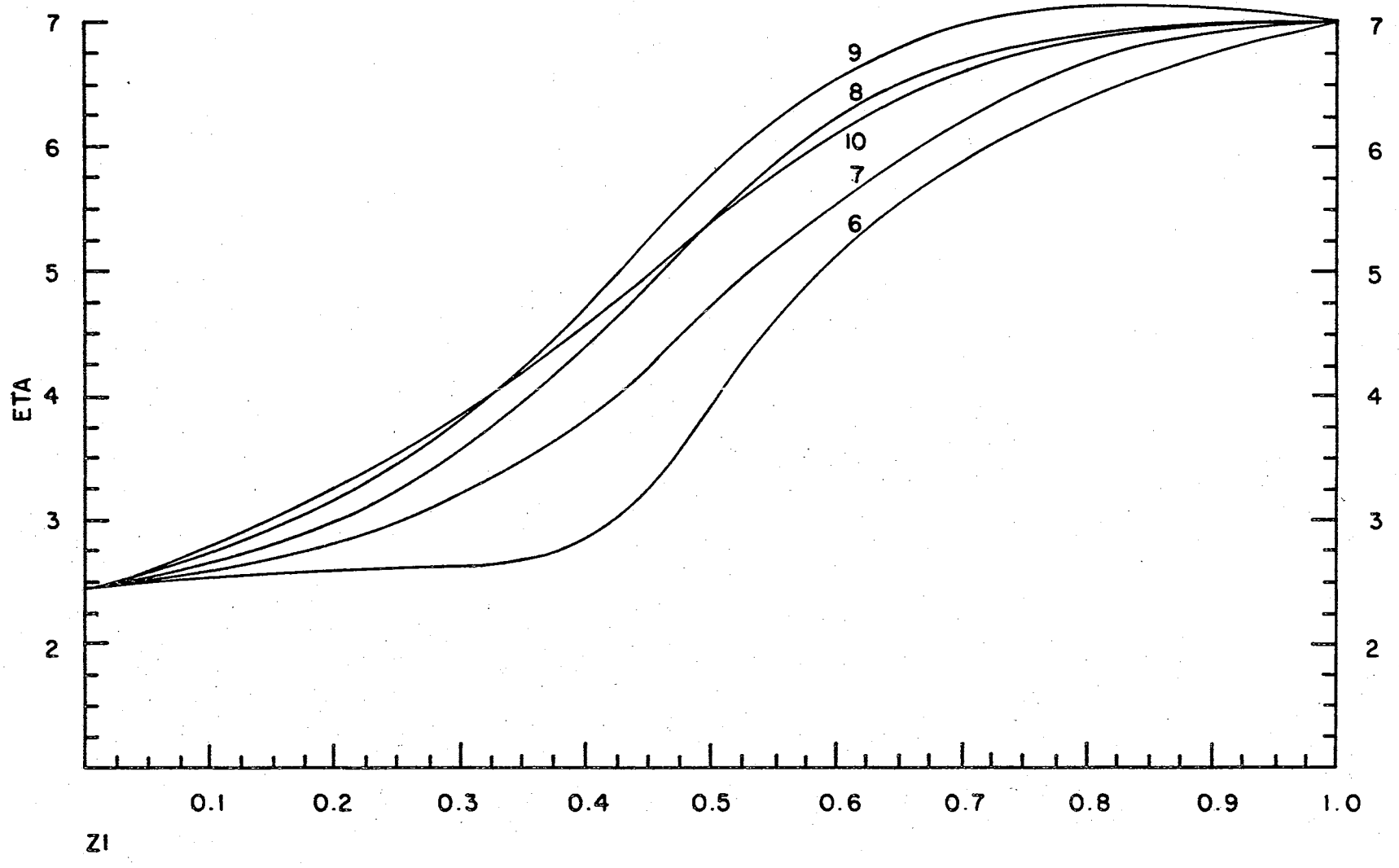

Figure 5. ^{5}L Term, f^{6} Configuration

5, and 6 levels arising from the ^5G term. As the figure indicates, Russell-Saunders coupling is a poor approximation for this term for any value of Zi. The order of the levels is badly distorted for all Zi values, but the graphical and experimental Etas of the J = 2 level agree to within the ability of the author to read the graph. It is felt, though that the assignment is correct, because of the close agreement with the experimental values for the $^5D_2$ level. Also the next J = 2 value lies more than one Eta unit higher.

Figures 7, 8, and 9 indicate the assignments of the levels arising from the ^5H, ^5I, and ^5F terms. They are so closely spaced that it is highly likely that incorrect assignments have been made, particularly since they have so many J-values in common. All three terms are badly J-mixed from the start, as would be expected from the close coincidence of so many common J-values. Since LS coupling is probably not a good approximation for any Zi value at this high an energy level, the main utility of these figures is probably to give the reader an idea of what happens at even higher values where the density of states is much greater.

The f^8 Diagrams

The Eta = 0 level can accept J-values of 0, 2, 4, and 6, so these values were assigned from levels arising from the ^7F multiplet of the f^8 configuration (Figure 10). The

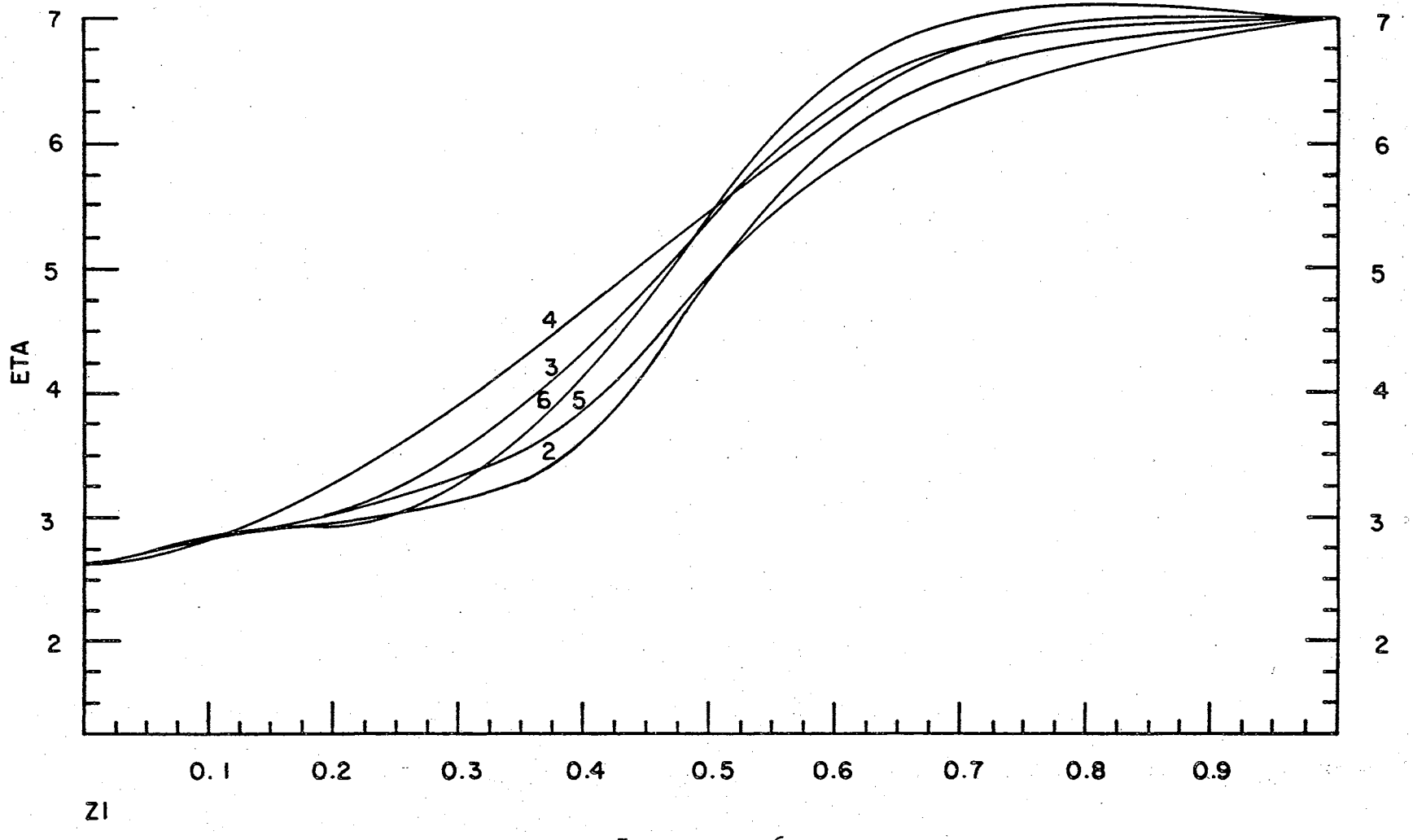

Figure 6. ^5G Term, f^6 Configuration

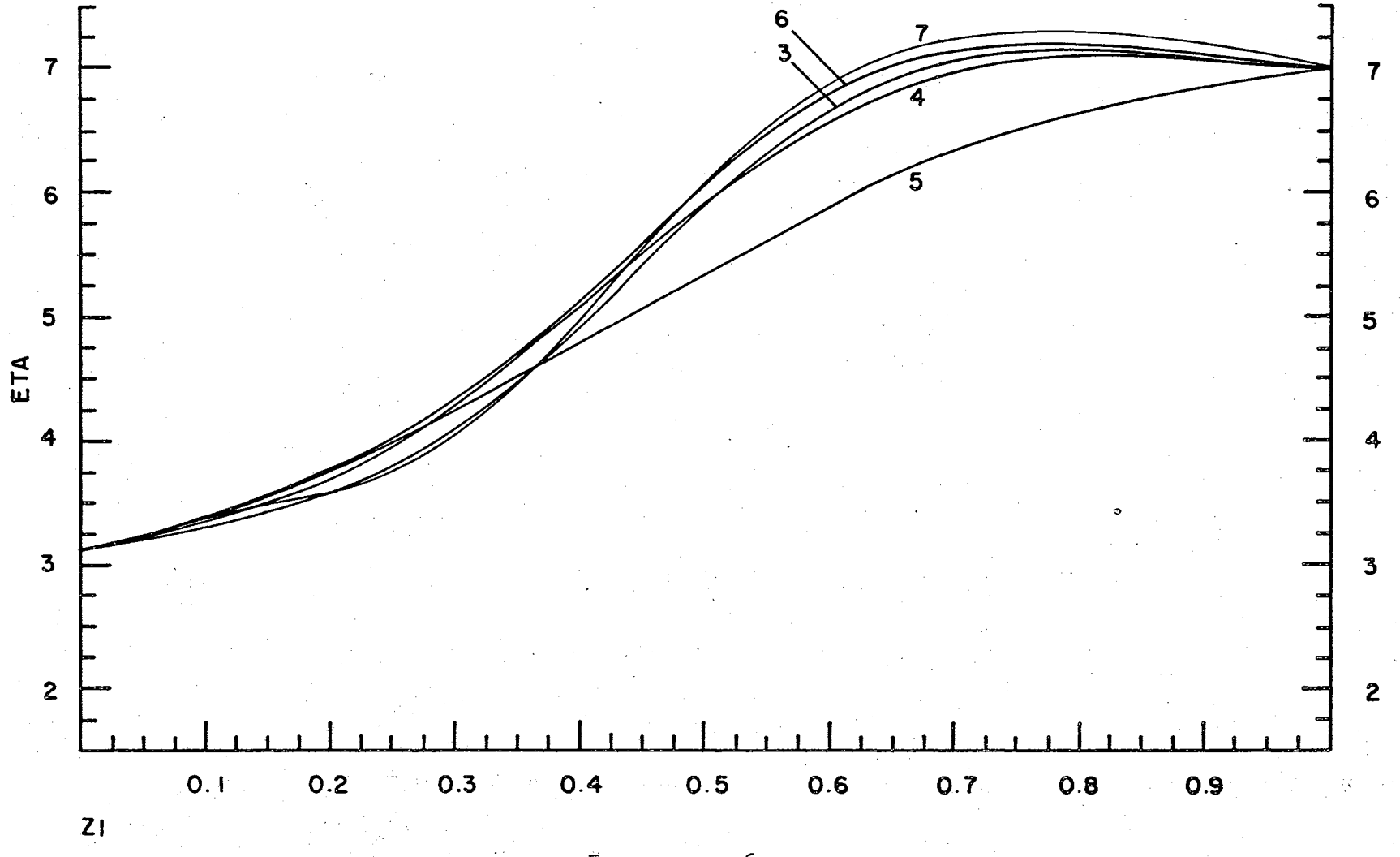

Figure 7. ^{5}H Term, f^{6} Configuration

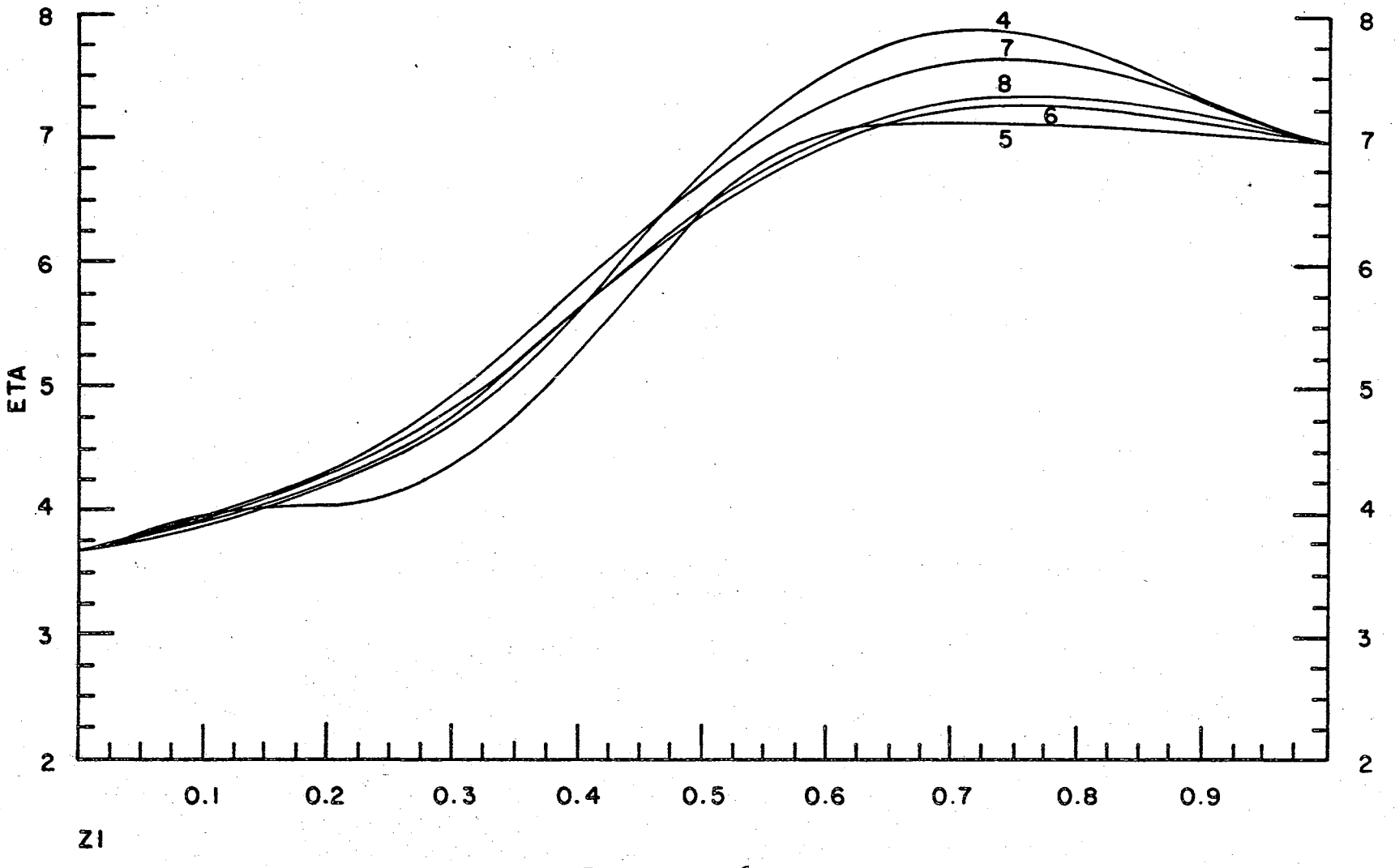

Figure 8. ^5I Term, f^6 Configuration

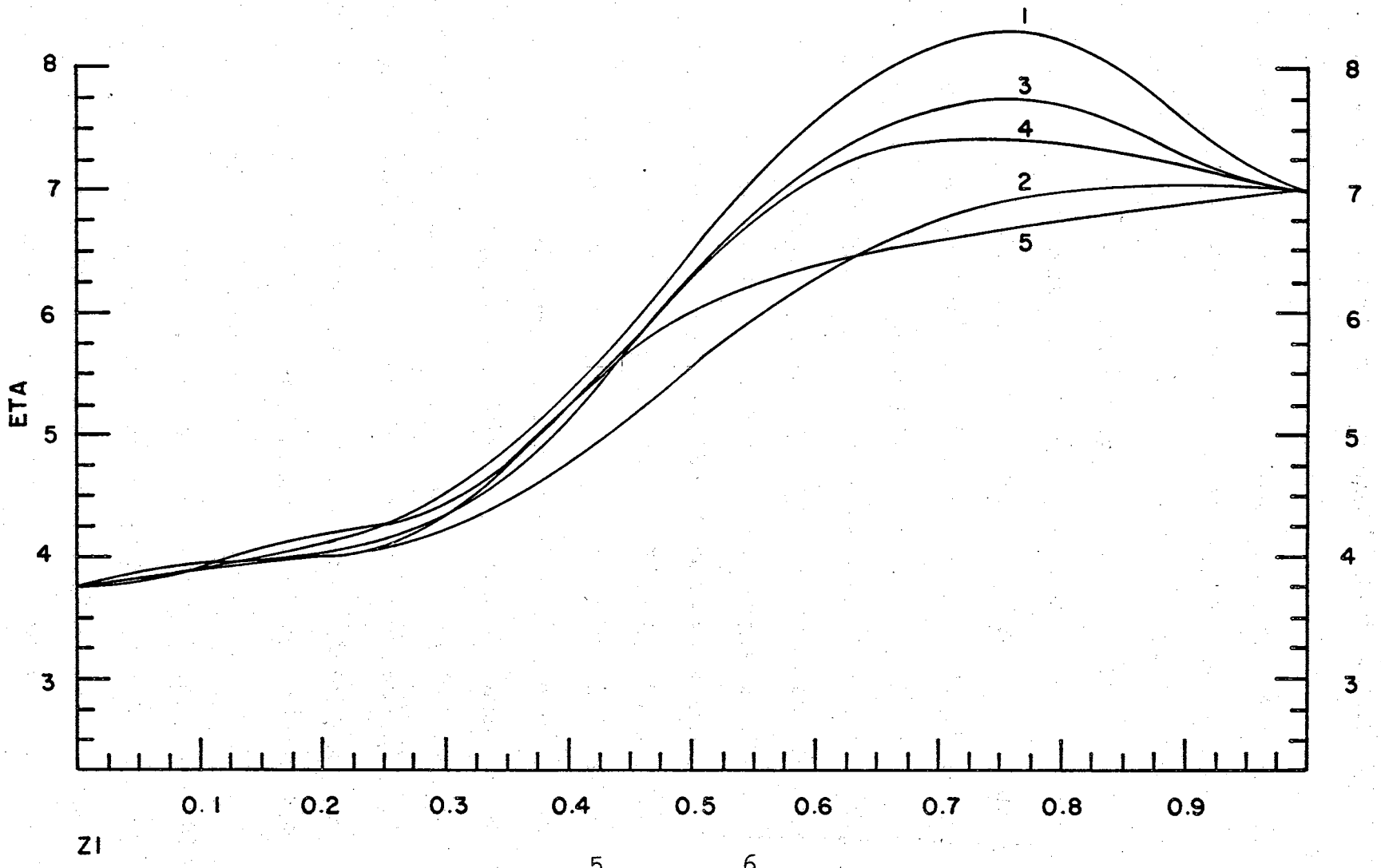

Figure 9. ^5F Term, f^6 Configuration

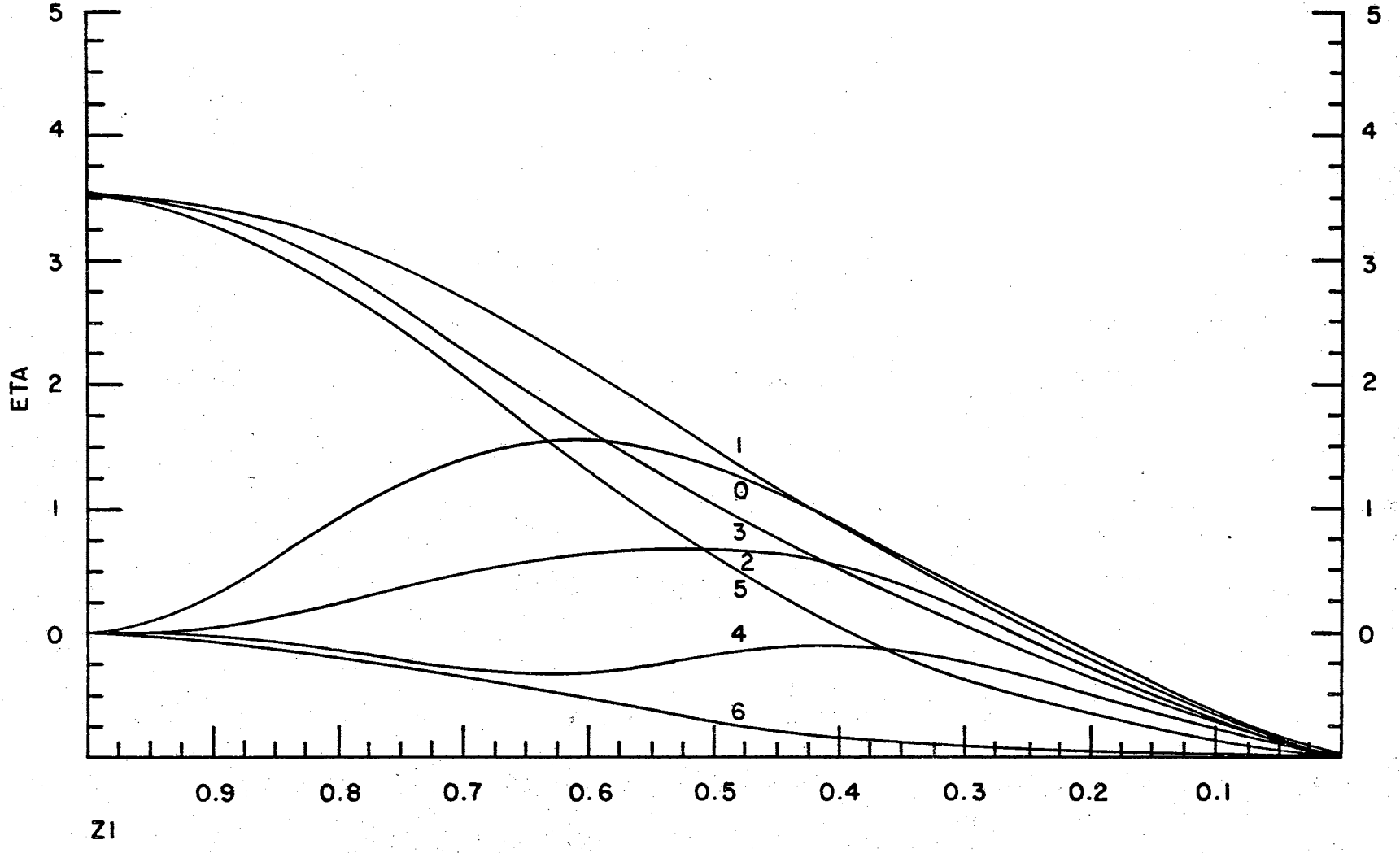

Figure 10. ^{7}F Term, f^{8} Configuration

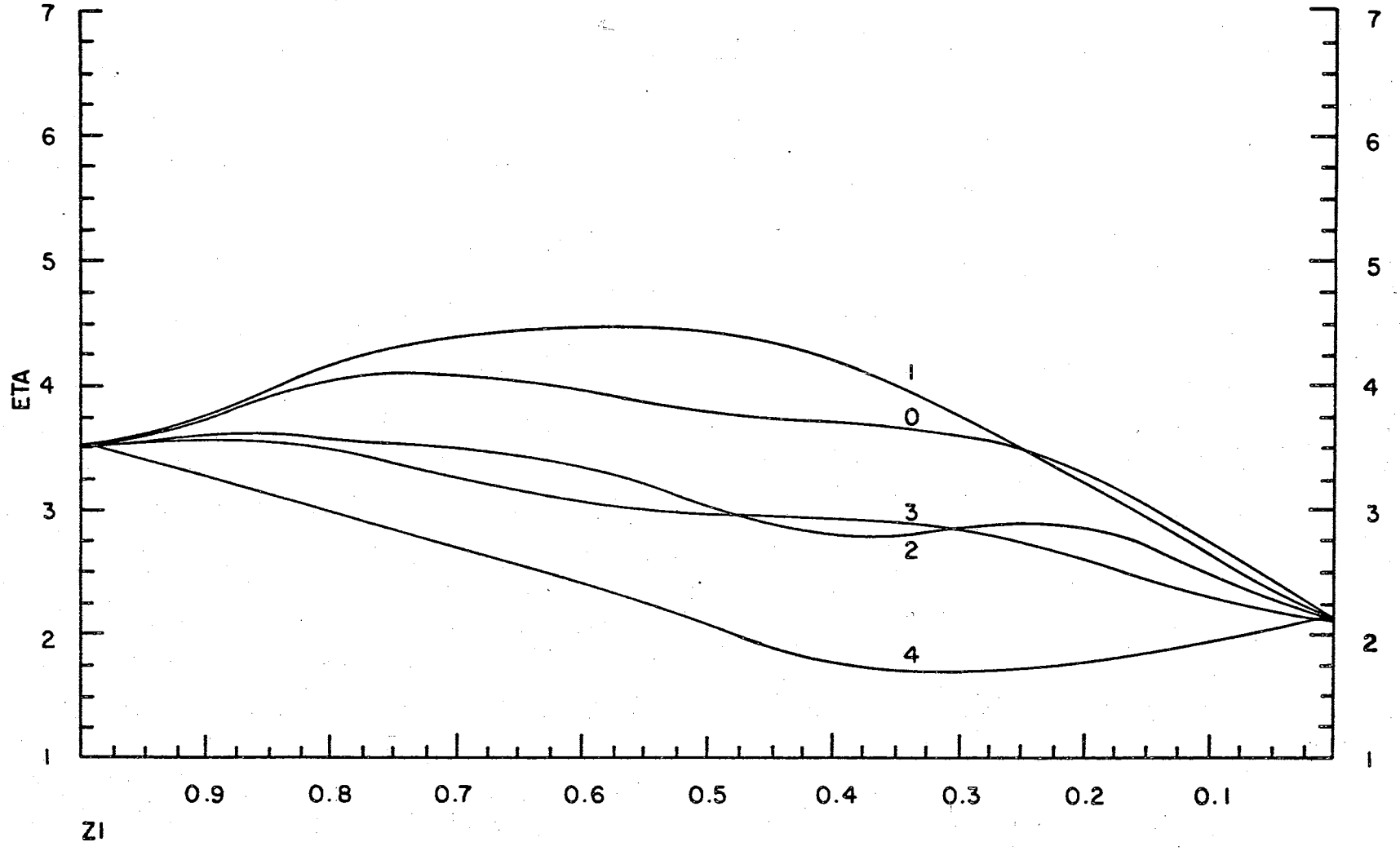

Figure 11. ^5D Term, f^8 Configuration

fit the levels better. J-values of 2, 3, and 4 are common to the ^5D and ^5G terms, and the lower set was assigned to the ^5D term and the higher to ^5G.

One of the more interesting features of the ^5G term in Figure 13 is the J = 6 level. At about Zi of 0.4, it becomes lower than the J = 4 level arising from the ^5D term. Since the region from Zi = 0.3 to 0.4 encompasses most of the ionization states of the actinides, it will be interesting to see if this behavior is corroborated by the experimental spectra. It should be mentioned that the way the levels are assigned, the J = 6 curve for the ^5L term is higher than that of the ^5G term, for most Zi values, even though the ^5L term is lower for the Russell-Saunders limit. At any rate, the Russell-Saunders scheme of labeling levels is of questionable value, since the calculations performed for these figures show that these levels are badly J-mixed for most values of Zi.

Figures 12, 14, 15, and 16 display the assignments of the J-levels arising from the ^5L, ^5H, ^5I and ^5F terms. They overlap to a large degree and again, some of the assignments are probably incorrect. They serve to satisfy 33 of the 34 J-values which terminate at the Eta = 3.5 level. The next highest term in the LS limit which can provide the missing J = 4 value is a ^5G term at Eta = 4.7, but there are several more before Eta = 5.0.

To summarize, 37 of the 38 possible levels terminating at either Eta = 0 or 3.5 in the jj limit have been assigned

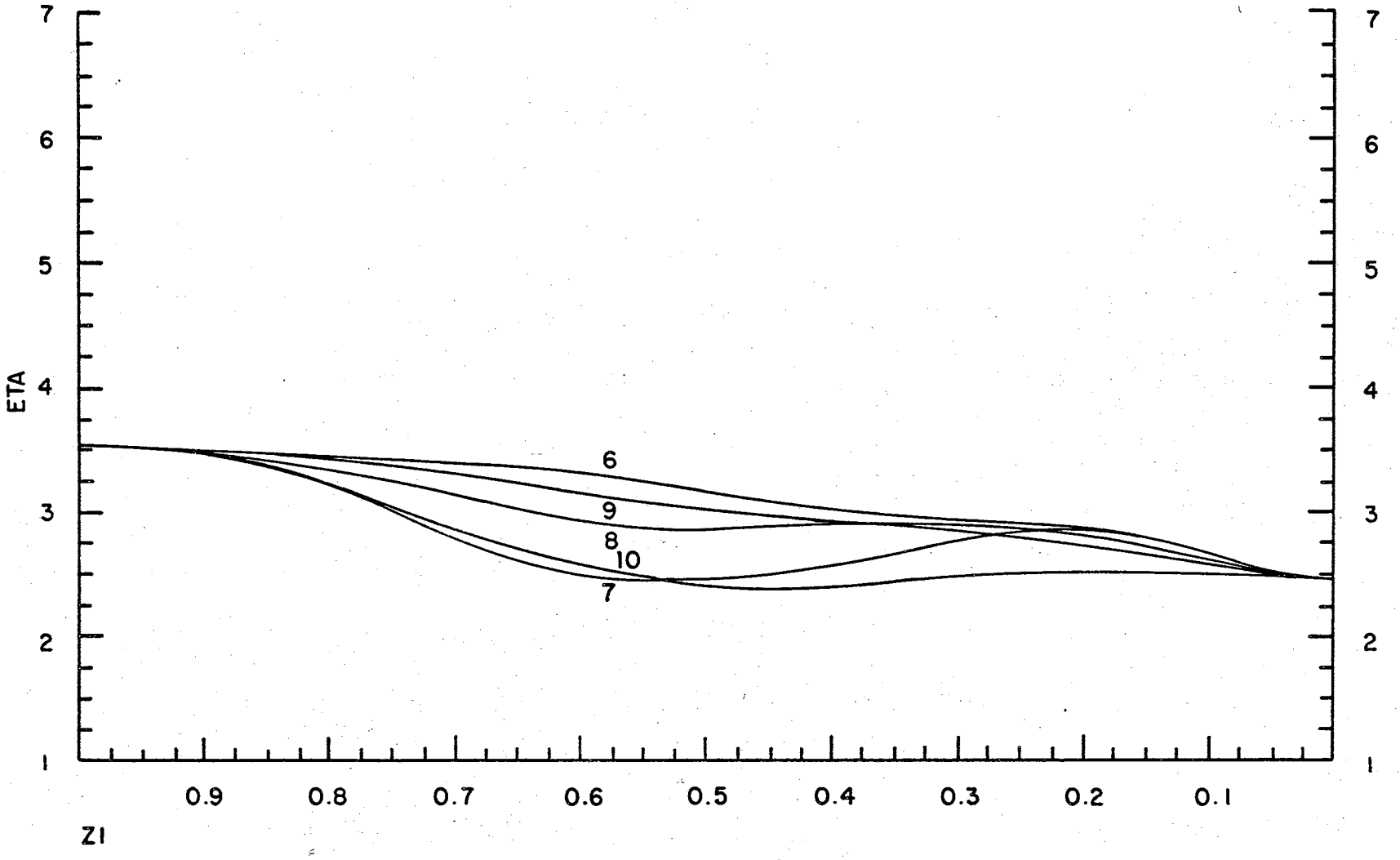

Figure 12. ^{5}L Term, f^8 Configuration

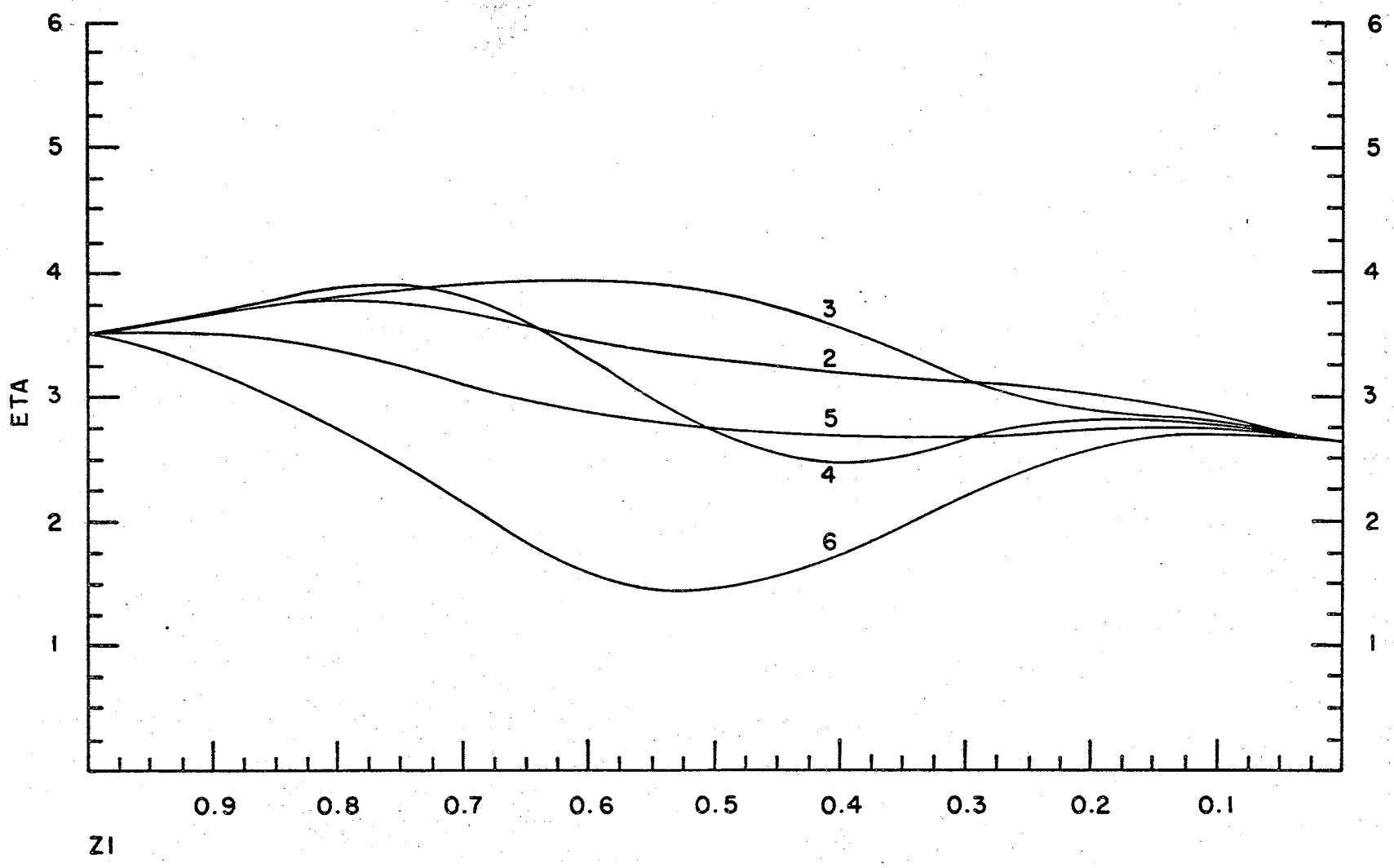

Figure 13. ^5G Term, f^8 Configuration

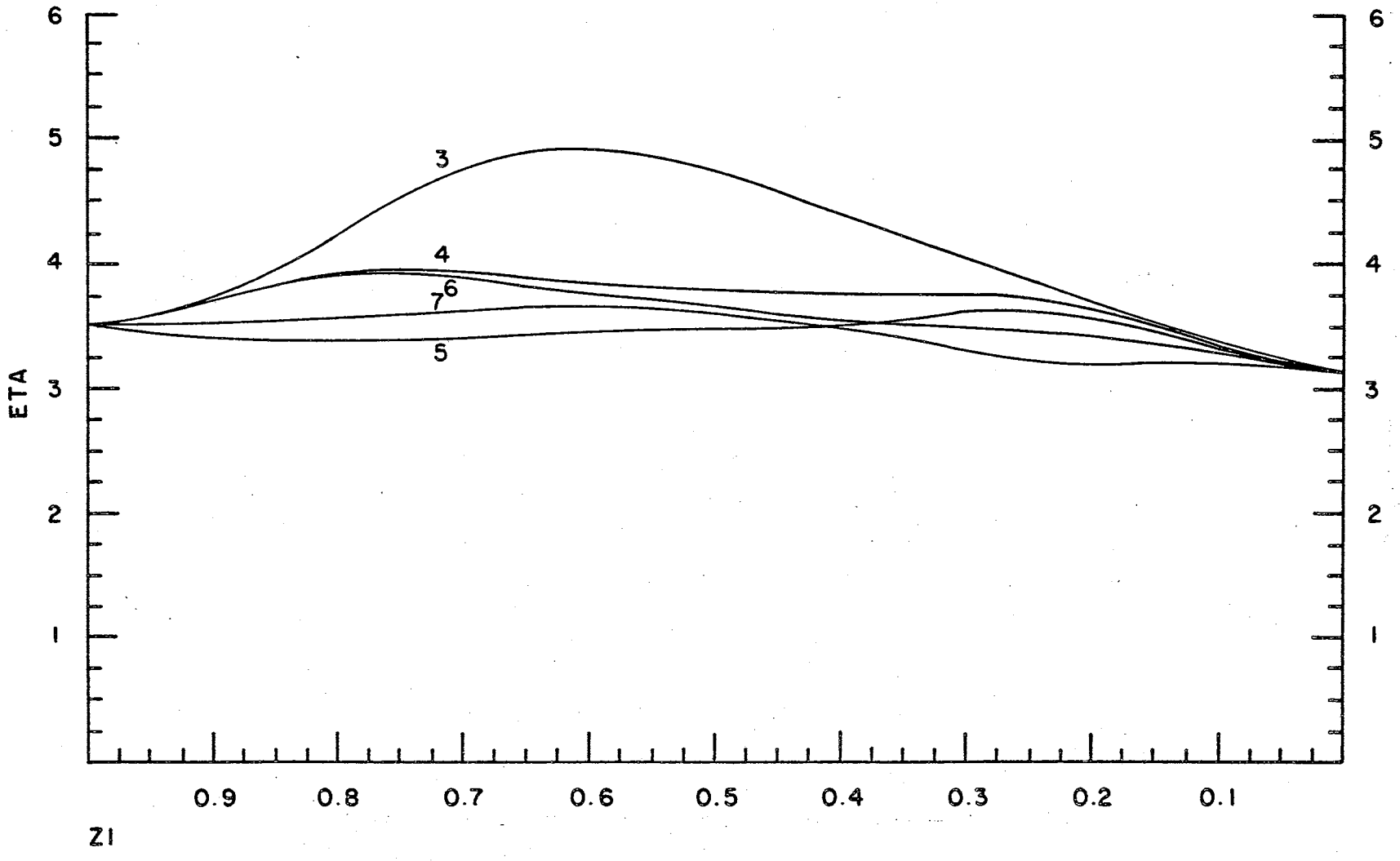

Figure 14. ^{5}H Term, f^{8} Configuration

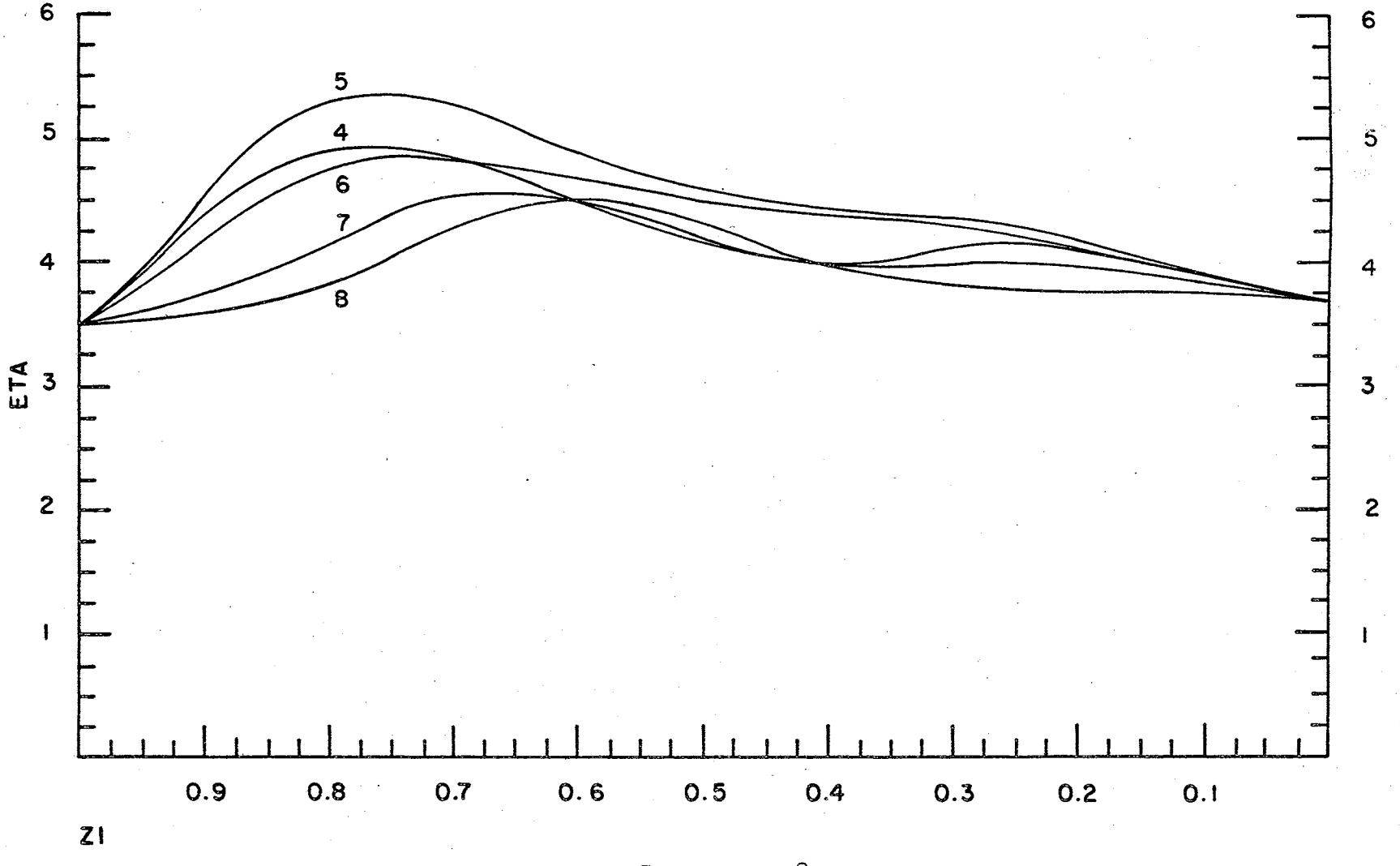

Figure 15. ^{5}I Term, f^{8} Configuration

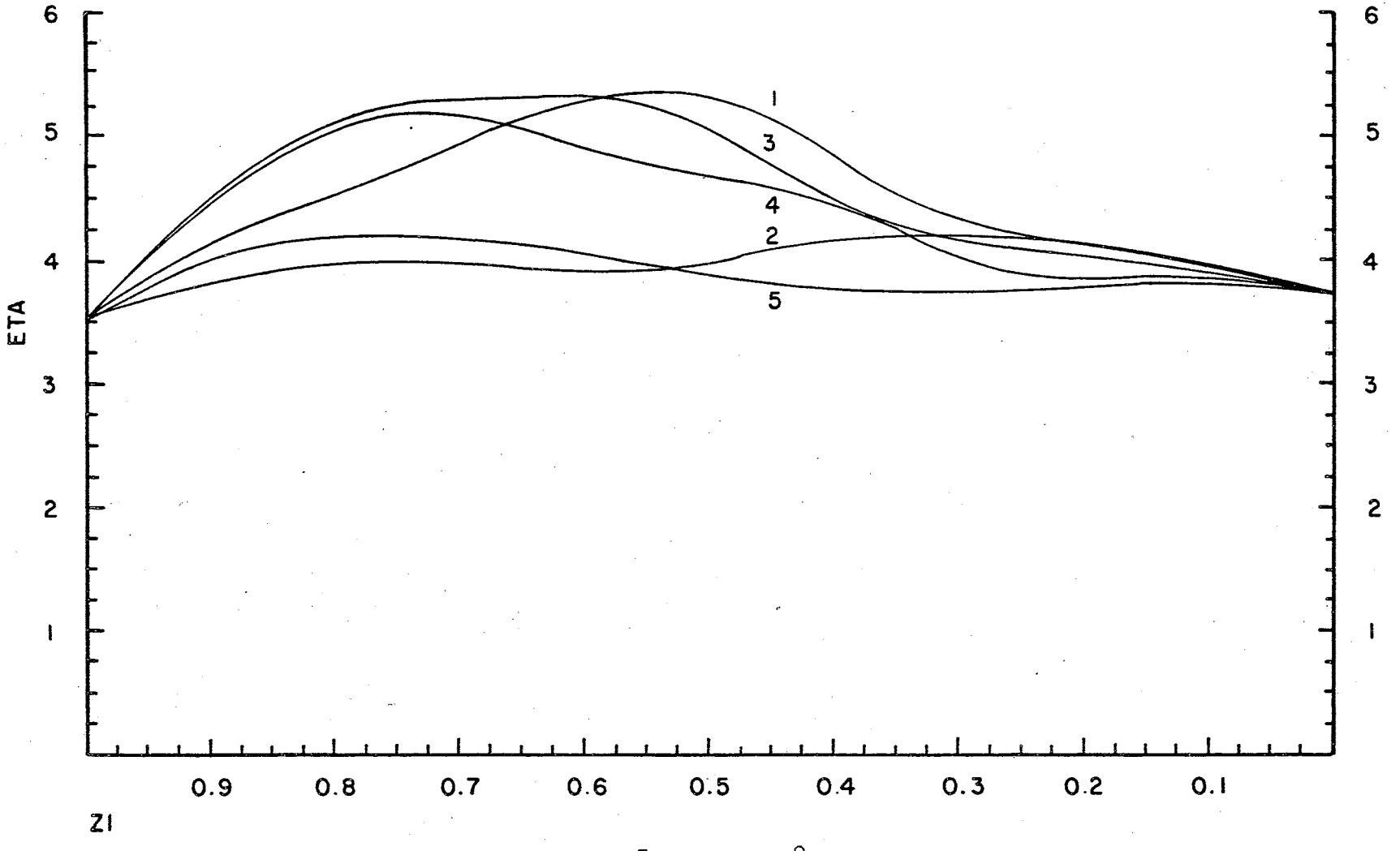

Figure 16. ^5F Term, f^8 Configuration

for the f^8 configuration. As there was a gap in terms at the LS limit, and since the next jj limit Eta level required 100 J-values, with only the highest J-values being easily assignable, no more figures were constructed. The same 37 J-values were also assigned to the three lowest eta levels in the jj limit for the f^6 configuration. Quite satisfactory agreement between the figures and two sets of energy levels for actinides in very different ionization states was obtained.

The High Levels of the f^6 and f^8 Configurations

As was previously stated, Figure 17 was constructed not so much in the belief that the levels represented the true behavior of the configurations, but in the hope that the relative spacings might be useful to spectroscopists. If two Eta values are subtracted from one another, for a particular value of F_2 and Zeta, the Eta expression reduces to

$$\Delta E = \Delta Eta((F_2/0.06)^2 + (Zeta)^2)^{\frac{1}{2}} \quad .$$

Figure 17 was initially constructed under the premise that the theory of Hund (30), previously mentioned, was operable. That is, levels of the same J should not cross. As was previously stated, calculations for the jj limit of both configurations showed that the Eta = 21 level of the f^8 configuration should have a single J = 0 term, and the

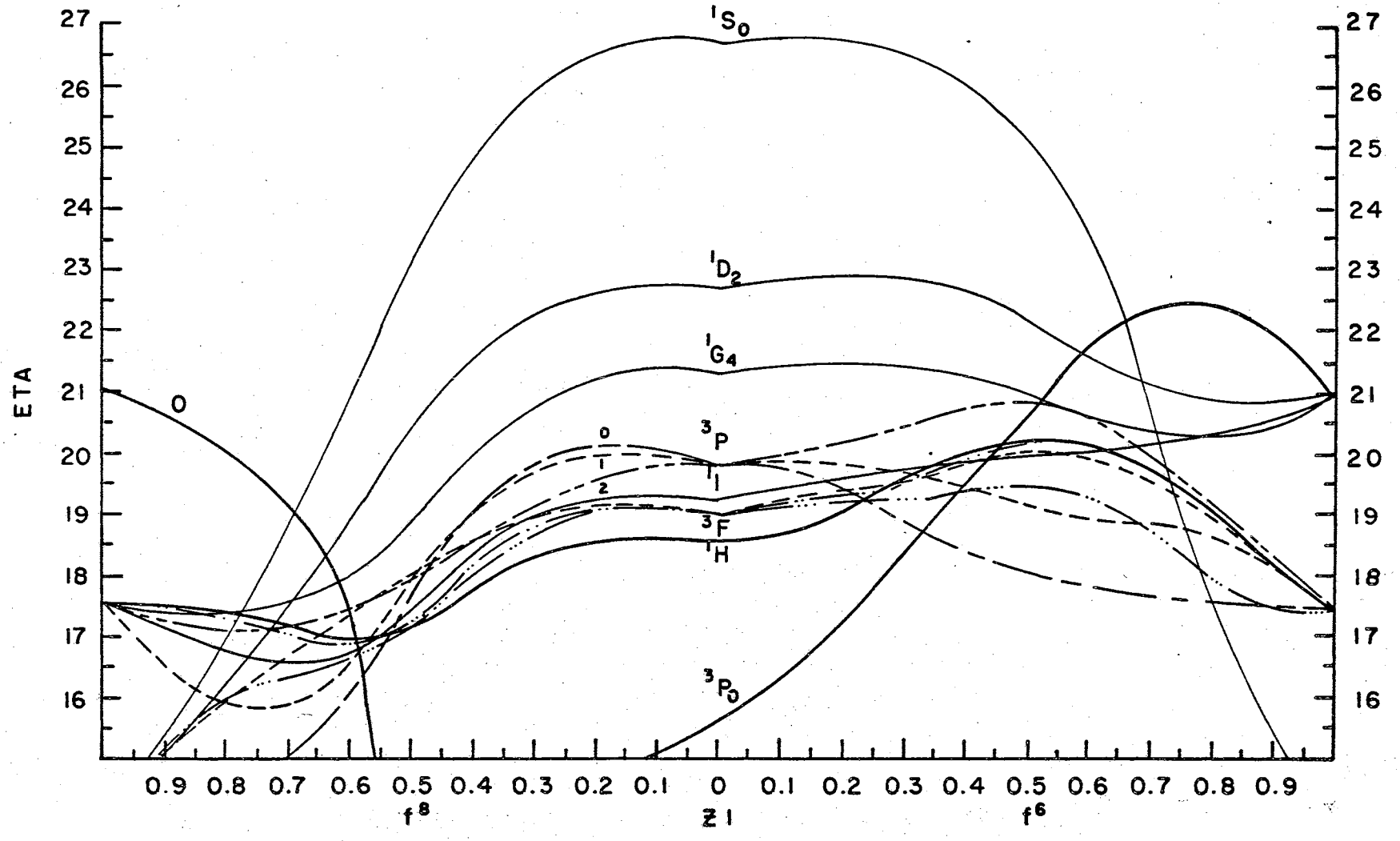

Figure 17. High Terms of the f^6 and f^8 Configurations

Eta = 17.5 level should have J-values of 1, 2, 3, 4, 5, and 6. For the f^6 configuration, J-values of 0, 2, 4, and 6 should terminate at the Eta = 21 level, and 34 J-values from 0 to 10 should terminate at the Eta = 17.5 level. Calculations at the LS limit showed the following terms present, in decreasing order: $^1S_0$, $^1D_2$, $^1G_4$, $^3P_{0,1,2}$, $^1I_6$, $^3F_{2,3,4}$, and $^1H_5$. Then there were a group of terms which were not plotted including, $^1G_4$, either ^3F or ^3H, $^1D_2$, $^3F_2$, and a closely spaced group which included a $^3P_0$ level which was plotted. Since the $^1S_0$ term was highest, it was assigned to the Eta = 21 level for both configurations. The $^1D_2$, $^1G_4$, and $^1I_6$ terms were assigned to the Eta = 21 level for the f^6 configuration and the Eta = 17.5 level for the f^8 configuration. This left only the ^3P and ^3F terms for assignment, because the $^1H_5$ level could be designated for Eta = 17.5 on both sides of the figure. The lower $^3P_0$ level was not chosen for assignment initially. The first hint of a problem was encountered when the next highest J = 0 level was plotted for the Zi values for which the computations were performed. For the f^8 configuration at Zi = 0.5, a J = 0 level was located slightly below Eta = 17.5, but for Zi = 0.75, a J = 0 level was found slightly above Eta = 17.5. Recalling that this level cannot accept a J = 0 term in the jj limit, this meant that if this level arose from the ^3P term, it had to make an extremely sharp turn downward past Zi = 0.75 in order to terminate at Eta = 14. When the f^6 configuration was

examined, the situation was the same, because even though the Eta = 17.5 level could accept one J = 0 value, there were apparently two levels in this region. At Zi = 0.35, the values were 18.5 and 18.8, at Zi = 0.5 they lay at 17.8 and 20.6, and at Zi = 0.75 the J = 0 levels were found at about 17.6 and 18.7. Clearly, another J = 0 level was rising from a lower Eta value to produce these effects, so the LS limit calculation was studied for a lower term with this property. The result was the $^3P_0$ level plotted at the lower part of Figure 17. This figure shows the way the J = 0 problem was resolved. By discarding the no-crossing rule, the $^1S_0$ level was terminated at Eta = 14, the higher $^3P_0$ level was terminated at Eta = 17.5, and the lower $^3P_0$ level was allowed to terminate at the Eta = 21 level. An alternate choice would have been to switch the final assignments of the two $^3P_0$ terms, and there are others, depending on which lower J = 0 term one wishes to invoke.

On the f^8 side of the figure, a similar solution was obtained. As finally constructed, the J = 0 term coming from off scale and terminating at Eta = 21 was drawn as arising from the lower of the two ^3P terms, but this need not necessarily be the case. The lower ^3P level could terminate at Eta = 14 and some still lower J = 0 level could rise to Eta = 21. This would produce a slope of the J = 0 curve between 0.5 and 0.75 which would not be as steep as the one shown in the figure. Similar problems with the J = 2 levels and the J = 4 levels were solved by assigning

the ^1D and ^3F terms to Eta = 14. The J = 4 level arising from the ^1G terms was assigned to Eta = 17.5 and the ^3F level to Eta = 14. As with the f^6 case, other solutions are possible, and the chances of this figure being entirely correct are extremely remote. The method of labeling the diagrams and levels according to the Russell-Saunders coupling scheme is merely a convenient way of giving the various levels a name, and nothing else is implied, particularly on this figure.

Other Configurations

As was stated in a previous section, the free ion levels for divalent cerium from reference 14 were least-squares fit and Eta and Zi values were calculated. Eta values for this configuration were plotted on the f^2 intermediate coupling diagram of reference 20, at a Zi value of 0.122. The agreement between the calculated Etas and the points on the curves was quite good, except for the previously mentioned problem of the $^1I_6$ level and the $^1S_0$ level. The f^2 intermediate coupling diagram indicates that the $^1I_6$ and $^3P_1$ levels cross over near this Zi value, so perhaps the $^1I_6$ level should have been retained. While the Eta value of the $^1S_0$ level did not come very close to the curve, neither did most of the other data points for this curve. Overall, the agreement between the Etas calculated for Ce III and the diagram were good. One particularly interesting aspect of the figure is the

comparison of the three $4f^2$ configurations, Ce III, Pr IV, and Nd V. The Zi value of praseodymium is 0.125, while that of neodymium is 0.159, indicating that there is a much larger deviation from Russell-Saunders coupling between the tetravalent and trivalent states than between the trivalent and divalent states.

The set of Eta values for the free-ion levels of Pr III from reference 15 were compared to the intermediate coupling diagram of the f^3 configuration (47). The Eta values were plotted at Zi = 0.124. The low-lying data points seemed to be consistently lower than the curves, averaging about 0.05 Eta units per level. This would indicate that a slightly higher value for F_2 would have given a better fit for the lower levels. On the other hand, the high levels fit very much better than the $^1S_0$ level of the f^2 configuration, so a higher F_2 would have improved the lower level fit only at the expense of the higher levels. The Zi value of trivalent neodymium is 0.136, indicating that the change from trivalent to divalent is a larger one for the f^3 case than it is for the f^2. The difference between the Zi values of the di- and trivalent states of the f^8 configuration is 0.011, compared to 0.012 for the f^3 configuration. This indicates that there may be something anomalous about the difference of only 0.003 for the f^2 configuration. On the other hand, the Zi interval of the di- and trivalent states of samarium and europium for the f^6 configuration is only 0.005, so there is probably

not enough experimental information to confirm any kind of trends with respect to this parameter. Using F_2 and Zeta values estimated from reference 20 for tetravalent promethium (f^3), a Zi of 0.169 can be calculated ($F_2 = 355$, Zeta = 1200), and the tetravalent-trivalent difference is 0.033, which compares very well with the f^8 difference, 0.035, and the f^2 difference, 0.034.

To summarize, the intermediate coupling diagrams of the f^6 configuration, and its conjugate case, the f^8 configuration have been constructed for the multiplets below 40000 cm^{-1} and compared to experimental information. In addition, free-ion spectra for two divalent cases have been recalculated and compared to intermediate coupling diagrams for their respective cases.

CHAPTER VII

CONCLUSIONS

The results of the experiments on reduction of the lanthanides in CaF_2 by electrolysis and irradiation were inconclusive, at best. The fact that the observed absorption in the visible and near-IR regions matched the published spectra indicated that some reduction occurred, but the fluorescence bands for the divalent f-f transitions were not observed, except for gadolinium. The absence of absorption bands for the same transitions was not particularly surprising, since most of the trivalent absorption bands which were observed were weak. Almost total reduction would have had to occur in order for some of the bands to be observed, and this was plainly not achieved. However, the fluorescence transitions should have been more easily observable, in spite of the lower concentration of the reduced ion, because of the broad, strong absorption bands available for pumping in the visible region. However, consideration of the absorption spectra of the reduced crystals indicates that fluorescence above about 10^4 cm^{-1}, the lower limit of the study, whould not appear, since for all the crystals except cerium and gadolinium, strong absorption bands, characteristic of f-d transitions, occur

at or below this energy. The cerium-containing crystals seemed to be impure or imperfect in some fashion, so the results are not surprising.

The observed fluorescence of the gadolinium must also be considered in the light of past studies. The ground state of Gd III has been found to be $4f^7 5d^1$ (18). Approximate calculations (8) for Gd(II) in CaF_2 indicate that there is a possibility that the same configuration is the ground state in the crystal. However, the f^8 configuration was not observed in the study reported by Callahan,[18] and in that paper, it was stated that the lack of observation indicated that this configuration was close to the $4f^7 5d^1$ configuration. Also, when the absorption bands observed in reference 32 are plotted on the same scale as (8), all the observed bands fell at the same energies. Divalent yttrium should have a $4d^1$ configuration, and it may be argued that this would be similar to the $4f^7 5d^1$ configurations because of the outer d electron, but the correspondence between Gd(II) and La(II) spectra, ($5d^1$), which, by this argument, should be even better, is not as good as that with Y(II).

A second possible explanation might be the mixing of the f^8 and $f^7 d^1$ configurations by the crystal field. A study (24) was made of the fluorescence and absorption of Sm(II) in CaF_2, BaF_2, and SrF_2. Fluorescence from the $^5D_0$ level on the f^6 configuration to the ground multiplet was observed for SrF_2 and BaF_2 at 14353 and 14374 cm^{-1},

respectively. For CaF_2, it was found at 14118 cm^{-1}, indicating a structure-sensitive shift which should not be found for the shielded 4f shell. This was confirmed by preparation of two crystals, one 98% CaF_2 and 2% SrF_2, the other 98% SrF_2 and 2% CaF_2. In the first crystal, the 14118 cm^{-1} line was shifted by 15 cm^{-1}, while in the second crystal, the line did not move appreciably from the energy observed in the pure SrF_2 crystal. Also, Zeeman studies showed that the fluorescence observed in the SrF_2 and BaF_2 crystals were magnetic dipole transitions, while for CaF_2 it was electric dipole in nature, which is forbidden for this system for f-f transitions. This evidence indicated that the fluorescent level was appreciably or perhaps predominantly 5d in character. A similar mechanism might be in operation for the gadolinium-doped crystals.

Good agreement was found between the intermediate coupling diagrams and the experimental levels for the f^6 and f^8 configurations. It is hoped that these figures will be an aid in further interpretation of free-ion and solid-state spectra which have already been studied, and in studies of higher ionization states which are still being carried out. Further studies of divalent lanthanides in alkaline earth fluorides should be carried out on crystals in which the interfering impurities are known to be absent or at negligible concentrations. Only then can the experimental results obtained in this and other studies be affirmed or refuted.

A SELECTED BIBLIOGRAPHY

(1) Dieke, G. H., and Crosswhite, H. M., Appl. Opt. 2, 675 (1963).

(2) Dieke, G. H., "Spectra and Energy Levels of Rare Earth Ions in Crystals," H. M. and Hannah Crosswhite, eds., Interscience, New York, 1968.

(3) Wybourne, B. G., "Spectroscopic Properties of the Rare Earths," Interscience, New York, 1965.

(4) Sinha, S. P., "Europium," Springer-Verlag New York, Inc., 1967.

(5) Asprey, L. B. and Cunningham, B. B., "Progress in Inorganic Chemistry," Vol. II, E. A. Cotton, ed., Interscience, New York, 1960.

(6) Fong, F. K., "Progress in Solid State Chemistry," Vol. 3, Pergamon Press, New York, 1967.

(7) Carnall, W. T., and Fields, P. R., "Advances in Chemistry," Vol. 73, R. F. Gould, ed., American Chemical Society Publications, Washington, D. C., 1967.

(8) McClure, D. S., and Kiss, Z. J., J. Chem. Phys. 39, 3251 (1963).

(9) Merz, J. L., and Pershan, P. S., Phys. Rev. 162, 217-47 (1967).

(10) Hayes, W., and Twidell, J. W., Proc. Phys. Soc. (London) 79, 1295 (1962).

(11) Sabisky, E., J. Appl. Phys. 36, 802 (1965).

(12) Kariss, Ya. E., and Feofilov, P. P., Opt. Spectry. 15, 308 (1963).

(13) Odabasi, H., J. Opt. Soc. Am. 57, 1459 (1967).

(14) Sugar, J., J. Opt. Soc. Am. 55, 33 (1965).

(15) Trees, R. E., J. Opt. Soc. Am. 54, 651 (1964).

(16) Dupont, A., J. Opt. Soc. Am. 57, 867 (1967).

(17) McElaney, J. H., J. Opt. Soc. Am. 57, 870 (1967).

(18) Callahan, W. R., J. Opt. Soc. Am. 53, 695 (1963).

(19) Bryant, B. W., J. Opt. Soc. Am. 55, 771 (1965).

(20) Varga, L. P., and Asprey, L. B., J. Chem. Phys. 48, 139 (1968).

(21) Nielsen, C. W., and Koster, G. F., "Energy Matrices for All Configurations of f Electrons," a magnetic tape prepared at MIT, Cambridge, Mass., 1962.

(22) Freeman, A. J., and Watson, R. E., Phys. Rev. 127, 2058 (1962).

(23) Herman, F., and Skillman, S., "Atomic Structure Calculations," Prentice-Hall, Inc., Englewood Cliffs, N. J., 1963.

(24) Wood, D. L., and Kaiser, W., Phys. Rev. 126, 2079 (1962).

(25) Loh, E., Phys. Rev. 154, 270 (1967).

(26) Rabbiner, N., J. Opt. Soc. Am. 57, 217 (1967).

(27) Judd, B. R., "Operator Techniques in Atomic Spectroscopy," McGraw-Hill Book Co., Inc., New York, 1963.

(28) Judd, B. R., Crosswhite, H. M., and Crosswhite, Hannah, Phys. Rev. 169, 130 (1968).

(29) Crosswhite, Hannah, Crosswhite, H. M., and Judd, B.R., Phys. Rev. 174, 89 (1968).

(30) Candler, C., "Atomic Spectra and the Vector Model," 2nd ed., D. Van Nostrand Co., Inc., Princeton, N. J., 1964.

(31) Varga, L. P., and Asprey, L. B., J. Chem. Phys. 49, 4674 (1968).

(32) O'Connor, J. R., and Chen, J. H., Phys. Rev. 130, 1790 (1963).

(33) deJong, W. F., and Bouman, J., "General Crystallography," W. H. Freeman and Co., San Francisco, 1959.

(34) Fong, F. K., J. Chem. Phys. 41, 245 (1964).

(35) Weakliem, H. A., and Kiss, Z. J., Phys. Rev. 157, 282 (1967).

(36) Makovsky, J., Phys. Lett. 19, 647 (1966).

(37) Prener, J. S., and Kingsley, J. D., J. Chem. Phys. 38, 667 (1963).

(38) Pearson, W. B., ed. "Structure Reports," Vol. 22, p. 235, 1958.

(39) Guggengeim, H., and Kane, J. V., Appl. Phys. Lett. 4, 172 (1964).

(40) Stanley, E. C., Kinneberg, B. I., and Varga, L. P., Anal. Chem. 38, 1362 (1966).

(41) Barrett, J., Semi-elements, Inc., Saxonburg, Pa., personal communication, 1969.

(42) Loh, E., Phys. Rev. 147, 332 (1966).

(43) Sugar, J., J. Opt. Soc. Am. 53, 831 (1963).

(44) Ofelt, G. S., J. Chem. Phys, 38, 2171 (1963).

(45) Conway, J. G., J. Chem. Phys. 40, 2504 (1964).

(46) Bauche, J., Blaise, J., and Fred, M., Compt. rend. 257, 2260 (1963).

(47) Varga, L. P., Reisfeld, M. J., and Asprey, L. B. To be published.

(48) Kogelnik, H. and Porto, S. P. S., J. Opt. Soc. Am. 53, 1446 (1963).

APPENDIX A

OTHER STUDIES

Construction of a Ruby Laser

A ruby laser was constructed for use as a light source for Raman spectrography, with a 2.5-meter Jarrell-Ash grating spectrograph and Polaroid type 413 infrared-sensitive film used for detection. The three inch by $\frac{1}{4}$ inch diameter ruby crystal was purchased from Adolph Meller Co., and was positioned at one focus of an elliptic cavity. At the other focus was an E.G. and G. F x 42 Xenon flash tube for optical pumping of the crystal. The resonant cavity of the laser was formed by two 99.8% reflecting, dielectric coated spherical mirrors of 0.5 m. focal length. The cell, with end windows either perpendicular or at the Brewster angle, containing the liquid to be examined, was placed within the resonant cavity of the laser, and the light which was scattered by the liquid was focused on the slit of the spectrograph.

The elliptical cavity had a major axis of $2\frac{1}{4}$ in. and a minor axis of 2 inches. It was fabricated from a split brass block by laying out the ellipse and, by a trial-and-error process, the number of cuts of a lathe which would remove the maximum amount of stock were determined. A

honing tool was ground to fit the curve of the ellipse at the point where excess stock remained. By this method, the variation of the cavity from the true ellipse was reduced to about one thousandth of an inch. Three successive lapping molds for final polishing of the ellipse were made by filling the cavity with Devcon 101 liquid epoxy. The first two molds were used with the cavity separated and the two pieces placed in line. The final polish was done with the cavity assembled. During each step, the mold was rotated and changed end-to-end to reduce the residual ridges. After the final polish, the cavity and the end plates, to which the crystal and flash lamp would be attached, were given a final cleaning by ionic bombardment in a vacuum system, and then coated with aluminum by vapor deposition.

A Westinghouse 2 KW industrial RF generator was modified to obtain a variable DC voltage source with a maximum output of about 3000 volts. The variable voltage was used to charge a 420 microfarad capacitor bank which was wired so that four capacitances were available, in steps of 105 microfarads. The circuit was completed by a 395 microhenry aircore choke and the flashtube. To fire the laser, the capacitor bank was charged to the chosen voltage by the power supply and the flash lamp acted as open switch preventing discharge of the capacitors. A high voltage pulse to a fine wire wrapped around the lamp then ionized enough of the gas in the lamp to start conduction. The choke was included in the circuit to give the right discharge rate for

the lamp-capacitor combination. The voltage pulse was obtained by discharge of a capacitor through the primary of a step-up transformer, with the secondary windings providing the pulse. The switching of the circuit was accomplished either by a tap key or a thyratron trigger circuit.

Several configurations of the laser system were tried to maximize the amount of scattered light incident on the slit of the spectrograph. One such configuration was the positioning of the laser on another optical track, with the sample cell in front of the slit. Light collection in this case was accomplished by cylindrical or spherical lenses. A second configuration consisted of a set of 15 flexible fiber optics light guides arranged around the sample cell. The opposite ends were then positioned before the slit, and focusing of the light was provided by the lens system. Since a fairly high pulse rate was required, the crystal and flash cavity were cooled by flowing N_2 gas through a coil immersed in a dry ice-ethanol bath and then directly into the flash cavity. To prevent condensation of water on the cooler components, the whole system was enclosed in a large polyethylene glove bag. Since the dry N_2 gas was vented directly into the bag, this provided a very effective barrier to condensation and allowed the laser to be triggered as many as 200 times in a reasonable period.

Reference lines were obtained from an iron arc spectra which was recorded on each piece of film. After arranging

the components in what was considered to be the optimum configuration, the laser was triggered 200 times for two separate exposures. No lines were ever observed in any of these studies, except for the excitation line of the laser and some regularly spaced lines of equal intensity on either side of the ruby line, which were determined to be grating ghosts produced by the high intensity of the laser pulse. In this region of the spectrum, the dispersion of the spectrograph was found to be about 23 wavenumbers per mm on the plate, so this should have been sufficient to remove the Raman lines of CCl_4, which should be displaced from the ruby line by 218, 314, 458, 762, and 791 cm^{-1} (48), from the intense clouding of the ruby line. No indication of lines at these positions was ever noted. It was finally determined that inefficient light collection or low power of the laser resulted in the absence of observed spectra.

Self-Consistent Field Calculations

A Hartree-Fock-Slater self-consistent atomic field program (23) was obtained for the purpose of calculating the radial electronic distributions for some configurations of the lanthanide ions. The input to the program consists of the nuclear charge of the atom or ion for which the calculation is to be performed, the charge on the ion, trial eigenvalues for each completely or partially filled shell in the configuration under examination, and a trial value for the potential in which the electrons move. The

program is not particularly sensitive to the trial eigenvalues used, and it has been found sufficient to use those for the neutral atom which are listed in reference 23 for each shell. The trial potential is the sum of the nuclear coulomb potential, the total electronic coulomb potentials, and an approximation to the electronic exchange potential. This approximation is given by the exchange potential for a free electron gas whose total electronic charge density is equal to that of the configuration under examination. The exchange potential has a total charge content of plus one unit, and has a magnitude at any value of r which is equal to the like-spin charge density at that point. This is a reasonable approximation at small values of r, but for larger values, it does not approach zero as it should. Therefore, the potential is redefined for values of $r \geq r_o$ so that $V(r) = -2(Z - N + 1)/r$, where Z is the nuclear charge, N is the number of electrons, and r_o is that value of r for which the free electron exchange potential is equal to $-2(Z - N + 1)/r_o$.

While the program will converge for a starting potential which is not very self-consistent, experience has shown that one cannot go too far. For instance, the potentials given in reference 23, for the neutral lanthanides worked satisfactorily for the di- and trivalent ions

derived from the same atom, but if the potential for the adjacent atom was used, the program would not converge. Although this problem was not encountered, it might also be true that the neutral potential would not be self-consistent enough if the calculation for a highly-charged ion was attempted. A method of circumventing this might be to perform the calculation for an intermediate ion, in order to obtain a starting potential which is closer to that required for the highly-charged ion.

The program requires a value for the potential at a specific number of points, usually every fourth point of the integration mesh. The listing in reference 23 does not always contain this many points, since it was truncated as soon as a limiting value was reached. Additional input cards may have to be added in order to attain the required number.

The integration and differentiation procedures in the program are written in terms of an integration mesh, with the potential function, $V(r)$, and the radial wave function, $P_{n\lambda}(r)$, represented by their values at the points of the mesh. The general operation of the program uses a 441 point mesh for the ground state and low-lying configurations, but highly excited states are better represented with a 481 or 521 point mesh. The units of the mesh are Bohr radii, and, in order to be able to represent all the atoms in the periodic table on a common scale, the units are reduced by a factor called the Thomas-Fermi parameter.

The relation is given by $r = \mu x$ where

$$\mu = (\tfrac{1}{2})(3\pi/4)^{2/3} Z^{-1/3}$$
$$= 0.88534138 Z^{-1/3}$$

In the program, the results are displayed in terms of the x parameter and a conversion table is printed to convert back to regular Bohr radii.

The 441 point mesh is divided into 11 blocks of 41 points each, with each block consisting of 40 equally spaced intervals. $\Delta X = 0.0025$ units in the first block and the interval is doubled in each succeeding block. This allows the potential and radial wave functions to be represented at closely-spaced intervals near the nucleus, where they change rapidly, and at wider distances farther from the nucleus where they are exponentially damped.

Using the starting values for the potential and the eigenvalues, the wavefunction is generated and the Schroedinger equation is solved for each orbital in turn in a subroutine. Then the potential is modified by one of a number of procedures, and the process is repeated. When the test for self-consistency is satisfied, the procedure is terminated and the output information is transferred to magnetic tape. Another program prepares the output information for display in the format of reference 23. The first part of the output consists of a table for conversion of the units of the integration mesh to Bohr radii. The final potential as a function of the integration mesh is

displayed next, and then the numerical value of the radial wavefunction for each shell as a function of the integration mesh is given. The display is condensed so that the value for every fourth point of the integration mesh is shown. At the start of the listing for each shell, the configuration for that shell and the eigenvalue are given. The main program does not take the multiplet structure of partially-filled shells into account, but corrections to the energy of each shell for relataivistic and spin-orbit effects can be obtained by use of another subroutine.

A plot of the square of the radial wave functions of the 4f, 5s, 5p, and 5d shells of divalent gadolinium as a function of the radius in Bohr units is displayed in Figure 18. The additional nodes of the 5s, 5p and 5d orbitals between about $r = 0.8$ and $r = 0$ have not been displayed in this figure. The indicated ionic radius of trivalent gadolinium was given by Dieke (2), and the 90% of charge point was obtained from integration and summation of the total charge of each orbital.

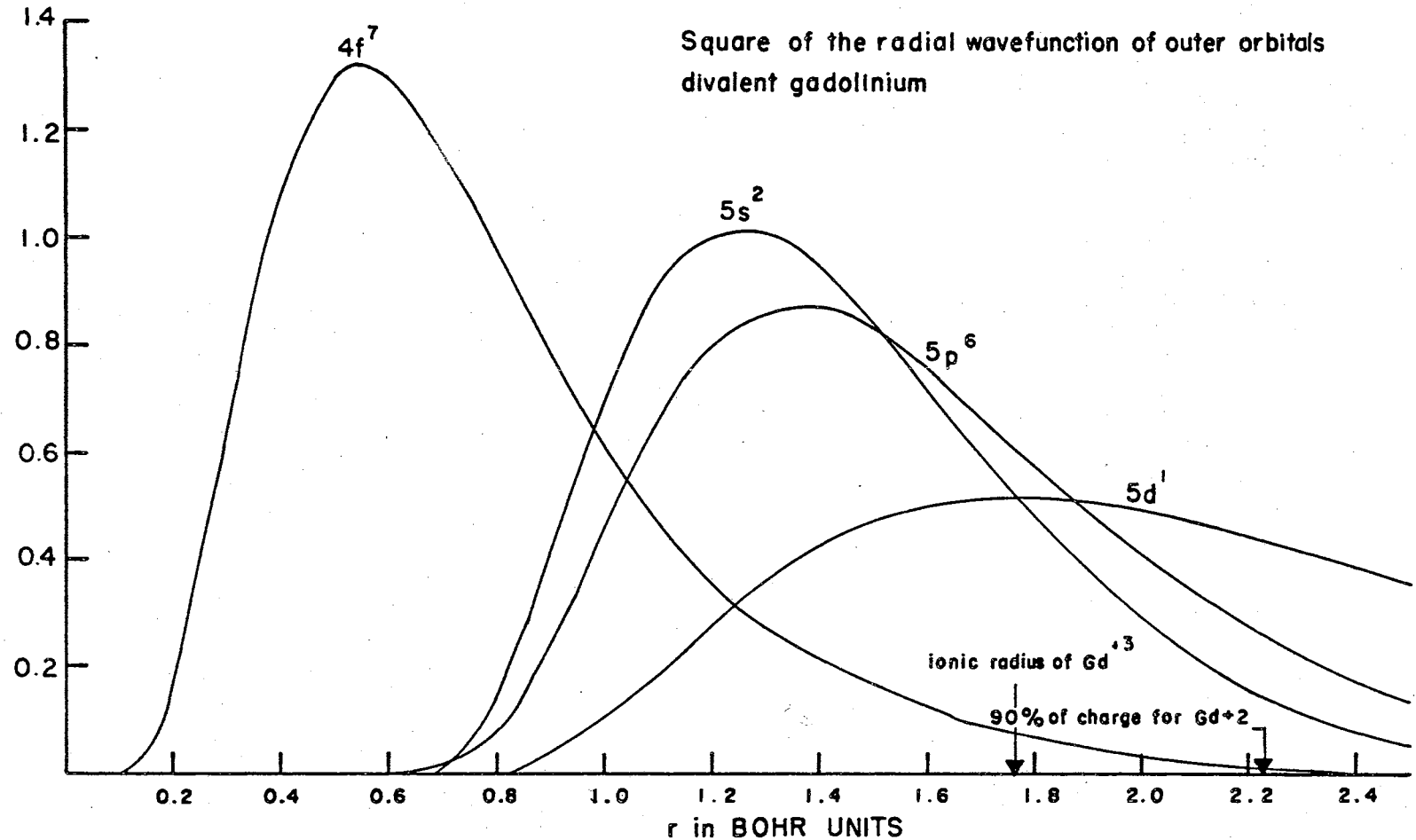

Figure 18. Square of the Radial Wavefunctions of the Outer Orbitals of Divalent Gadolinium

APPENDIX B

SPECTRA OF DIVALENT RARE EARTHS IN CALCIUM FLUORIDE AND CALCULATION OF ENERGY LEVELS OF THE f^6 AND f^8 CONFIGURATIONS IN INTERMEDIATE COUPLING

Abstract

Absorption studies of Ce(II), Pr(II), Gd(II), Ho(II) and Er(II) in CaF_2 were performed from 40000 cm^{-1} to 900 cm^{-1} on samples reduced by Co^{60} gamma radiation or solid-state electrolysis. Emission studies were performed on electrolytically reduced samples from 40000 cm^{-1} to 10000 cm^{-1}. In addition to previously reported spectra, new bands were observed at 27800, 32000, 39500, and 43000 cm^{-1} for Ho(II), and at 29200 and 32600 cm^{-1} for Er(II). A weak fluorescence peaking at 15000 cm^{-1} was observed in the Gd-doped crystals. Calculations were performed on all the available f^n configuration, free-ion energy levels of the divalent lanthanides in order to obtain the variation in F_2 and Zeta with the number of f electrons. This information was used to propose an interpretation of the fluorescence of the Gd-doped crystal. The intermediate coupling diagrams for the seven lowest

and seven highest terms of the f^6 and f^8 configurations were constructed for the transition from Russell-Saunders to jj coupling.

Introduction

Survey studies of all the lanthanides in CaF_2 have been reported for reduction by gamma irradiation (8, 9), and detailed studies of particular rare earths have also been published (10, 11, 12). Some of the divalent lanthanides have also been produced by solid-state electrolysis (6, 35, 39). When a CaF_2 crystal, doped with the lanthanide fluoride, is heated to 600-700°C and a DC potential is applied across the faces of the crystal, reduction of the dopant to the divalent state occurs. Since fluorides are the predominant charge-carriers in the lattice, the electrical field probably causes the interstitial charge-compensating fluorides to migrate toward the anode, making the trivalent lanthanides at a divalent cation site available for reduction (6). The divalent state produced by this method appears to be stable to ordinary temperatures and wave lengths of light. In contrast, the radiation induced coloration is unstable, and emission characteristic of the trivalent lanthanide is observed upon warming of the crystal, which frees the holes produced during irradiation. The holes migrate through the crystal and recombine with the electron at the reduced lanthanide. Furthermore, only a small percentage of the lanthanide ions

are reduced by gamma radiation. The thermoluminescence which is observed on heating is characteristic of a trivalent ion at a cubic site, so only those ions which are not locally compensated by an interstitial fluoride are capable of being reduced by this method (9).

Various schemes have been proposed for aid in the identification of free-ion or condensed phase spectra which deviate from Russell-Saunders coupling (2, 28), where the spin-orbit interaction cannot be neglected. Varga and Asprey (31) have proposed a pair of functions, dependent on the electrostatic parameter, F_2, and the spin-orbit coupling parameter, Zeta, which give the variations of the energy levels of the f^n configuration from pure Russell-Saunders to pure jj coupling. These functions have been used to obtain the intermediate coupling diagrams for the f^6 and f^8 configurations.

The present paper involves absorption and fluorescence studies of some divalent lanthanides in CaF_2 produced by electrolylic or radiation reduction techniques. The variation of F_2, the electrostatic interaction parameter, and Zeta, the spin-orbit coupling parameter, with the number of electrons in the 4f shell has been obtained. The intermediate coupling diagrams for the seven lowest and seven highest terms of the f^6 and f^8 configurations have also been constructed.

Experimental

Single crystal CaF_2 chips were purchased from Semi-elements, Inc., (Saxonburg, Pa.). The nominal concentrations of Pr, Gd, Ho, and Er were 0.1 mole percent, and the Ce concentration was 0.25 mole percent. The unreduced Ce-doped crystals were unstable to heat and had visible inclusions. The Pr-doped crystals contained Ce(III) as an impurity and the Gd-doped crystals contained Eu(III). Absorption spectra of the crystals before and after reduction were obtained from 40000 cm^{-1} to 4000 cm^{-1} on a Cary 14 spectrophotometer at 77°K, and from 4000 cm^{-1} to 900 cm^{-1} on a Beckman IR-7 at room temperature. Fluorescence spectra of the crystals before and after electrolytic reduction were obtained on a Farrand spectrofluorometer from 40000 cm^{-1} to 10000 cm^{-1} at 77°K. Electrolytic reduction of the crystals was performed in a fashion similar to that of Guggenheim and Kane (39), in a dry argon atmosphere. Irradiation of the crystals was accomplished at room temperature in a Gammacell 200 (Atomic Energy of Canada, Ltd.) Co^{60} source. The crystals were exposed to a total dosage of 2×10^6 rads.

Results and Discussion

No absorption bands were observed in the radiation-reduced Ce-doped crystals which had not been previously reported (8). Because of the instability of these crystals

to temperatures higher than about 400°C, no electrolytic reductions could be performed. The Pr-doped crystals also exhibited no bands not previously reported, as was true for the Gd-doped crystals, In addition to the previously-reported bands for Ho(II) in CaF_2, additional peaks were observed at 27800, 32000, 39500, and 43000 cm^{-1}. For the Er(II)-doped crystals, additional bands at 29200 cm^{-1} and 32000 cm^{-1} were observed in absorption.

Fluorescence studies of the electrolytically-reduced samples yielded a single line at 15000 cm^{-1} for the Gd(II)-doped crystal. All others gave only lines characteristic of the various trivalent ions. This emission could not be attributed to Eu(III), Sm(II) or to the f^7d configuration reported by Callahan (18) as the grond state of Gd III. The free-ion spectra of La III (13), Ce III (14), Pr III (15), Ho III (17), and Yb III (19) have been published and calculations, using the program described by Varga and Asprey (20), were performed on the reported levels of Ce III, Pr III and Ho III to obtain enough information to construct Figures 1 and 2. Using the value of Zeta (-1360 cm^{-1}) for the f^8 configuration from Figure 2, the value of F_2 in the program was varied until the energy difference between the $^5D_4$ level and the average of the $^7F_4$ and $^7F_5$ levels was equal to 15000 cm^{-1}. The value of F_2 obtained was 371 cm^{-1}. Wood and Kaiser (24) have reported a fluorescence line previously attributed to the $^5D_0$ level of Sm(II) as being substantially or perhaps

predominantly of d character, and a similar mechanism may be in operation here, but it would take a study similar to the one they performed to determine if this is the case. Also, the presence of other impurities cannot be ruled out.

Intermediate coupling calculations were performed at enough values of F_2 and Zeta to construct Figures 3 through 17. The ordinate for these figures is defined by the expression

$$\text{Eta} = \frac{E - \frac{F_2}{0.06}}{((F_2/0.06)^2 + \text{Zeta}^2)^{\frac{1}{2}}}$$

where E is the energy of the level, and F_2 and Zeta are the electrostatic and spin-orbit parameters. The abscissa is

$$\text{Zi} = \frac{0.06\ \text{Zeta}/F_2}{1 + 0.06\ \text{Zeta}/F_2}$$

for positive values of Zeta. For negative values of Zeta, Zi is defined by the expression

$$\text{Zi} = \frac{-0.06\ \text{Zeta}/F_2}{1 - 0.06\ \text{Zeta}/F_2}$$

since Zeta is negative for an f shell which is more than half full. As Zi varies from zero to one, the coupling goes from pure Russell-Saunders ($F_2 \gg$ Zeta) to jj (Zeta $\gg F_2$). The calculated values of Eta were not plotted on the figures in order to keep them as simple as possible, but good agreement was obtained between the figures and experimental values of some levels of Am IV and Pu I reported by

Conway (45) for the f^6 configuration, and for Dy(IV), of the f^8 configuration, reported by Varga and Asprey (20). These figures were constructed in the hope that they might aid spectroscopists in identification of more of the 295 levels of these configurations.

Acknowledgement

This work was supported in part by The Research Foundation of Oklahoma State University. We are indebted to George Gorin for the irradiation of the doped CaF_2 crystals.

VITA

William Beckham Volz

Candidate for the Degree of

Doctor of Philosophy

Thesis: SPECTRA OF DIVALENT RARE EARTHS IN CALCIUM FLUORIDE AND CALCULATION OF ENERGY LEVELS OF THE f^6 AND f^8 CONFIGURATIONS IN INTERMEDIATE COUPLING

Major Field: Chemistry

Biographical:

Personal Data: Born in Chickasha, Oklahoma, July 9, 1942, the son of Mr. and Mrs. W. J. Volz.

Education: Attended Fort Cobb Public Schools through eleventh grade; received the Bachelor of Science degree from Oklahoma State University in 1963, with a major in Chemistry; completed requirements for the Doctor of Philosophy degree in May, 1970, with a major in Chemistry.

Professional Experience: Graduate teaching assistant, 1966-68.

Member: Phi Eta Sigma, Omicron Delta Kappa, Phi Kappa Phi, American Chemical Society, Sigma Xi.